INFORMATION TO USERS

This dissertation was produced from a microfilm copy of the original document. While the most advanced technological means to photograph and reproduce this document have been used, the quality is heavily dependent upon the quality of the original submitted.

The following explanation of techniques is provided to help you understand markings or patterns which may appear on this reproduction.

1. The sign or "target" for pages apparently lacking from the document photographed is "Missing Page(s)". If it was possible to obtain the missing page(s) or section, they are spliced into the film along with adjacent pages. This may have necessitated cutting thru an image and duplicating adjacent pages to insure you complete continuity.

2. When an image on the film is obliterated with a large round black mark, it is an indication that the photographer suspected that the copy may have moved during exposure and thus cause a blurred image. You will find a good image of the page in the adjacent frame.

3. When a map, drawing or chart, etc., was part of the material being photographed the photographer followed a definite method in "sectioning" the material. It is customary to begin photoing at the upper left hand corner of a large sheet and to continue photoing from left to right in equal sections with a small overlap. If necessary, sectioning is continued again — beginning below the first row and continuing on until complete.

4. The majority of users indicate that the textual content is of greatest value, however, a somewhat higher quality reproduction could be made from "photographs" if essential to the understanding of the dissertation. Silver prints of "photographs" may be ordered at additional charge by writing the Order Department, giving the catalog number, title, author and specific pages you wish reproduced.

University Microfilms

300 North Zeeb Road
Ann Arbor, Michigan 48106

A Xerox Education Company

DETERMINATION OF THE RELATIONSHIP OF LUMINESCENCE AND PHOTOCONDUCTIVITY IN ZnS TYPE PHOSPHORS WITH MICROWAVE AND OPTICAL TECHNIQUES

by

Samuel Gelfman

A dissertation submitted to the Graduate Faculty in Physics in partial fulfillment of the requirements for the degree of Doctor of Philosophy, the City University of New York.

-1972-

This manuscript has been read and accepted for the Graduate Faculty in Physics in satisfaction of the dissertation requirement for the degree of Doctor of Philosophy.

5/15/72
date

Bernard Kramer
Chairman of Examining Committee

5/16/72
date

Warren A. Hirtleman
Executive Officer

Arthur Damask

James Freeman

Milton Furst

Kalman Kalikstein
Supervisory Committee

The City University of New York

To Laura, Michael and Dukie

ACKNOWLEDGMENT

I welcome this opportunity to express my sincere appreciation to Professor Bernard Kramer for the interest and active guidance he gave throughout this work. I am indebted as well, to Professor Kalman Kalikstein for his considerable contribution.

Moreover, I should like to tender my thanks to Mr. Paul Balkin, aided by Mr. Rubin Jordan and Mr. Michael Rubusch, for valuable technical assistance and to Mrs. Alice Forman for typing the manuscript.

TABLE OF CONTENTS

LIST OF TABLES

LIST OF FIGURES

I. Introduction

A. Properties of (Zn;Cd)S Phosphors

The luminescent properties of (Zn;Cd)S have been investigated over the past 100 years, beginning with Sidot in 1869. It is known that although pure, unheated ZnS is non-luminescent, it can be activated to luminescence by either the addition of impurities or by heating under various conditions. Common elements used for activation include copper, silver and manganese. Various energy levels and transitions have been proposed for the light emitting process, and a good deal of investigation continues in this field.

For a somewhat shorter period of time the photoconductive response of the ZnS family of materials has been under investigation not only because of the basic interest in photoconducting solids but as a way of understanding the electronic process involved. The photoconductivity has also been found to depend strongly on the type of activation.

Excitation of these materials can be carried out with visible or ultraviolet radiation, as well as electrons, α-particles, x-rays, γ-rays, etc. The use of infrared radiation (either during or after excitation) to stimulate (increase) or quench (decrease) the luminescent and photo-

conductive response was observed as early as 1920.

In the present experiment the luminescent and photoconductive characteristics of activated (Zn;Cd)S phosphors are simultaneously measured under various conditions of excitation. The photoconductivity of these phosphors is measured with a microwave bridge method[1] which is believed superior to other known methods.

The following review describes (a) some of the physical properties and (b) several phenomenological models that have been developed to explain the photoconductivity and luminescent properties of activated (Zn;Cd)S.

Crystal Structure: ZnS crystallizes in two forms, hexagonal (wurtzite) and cubic (zincblende). The former occurs when the firing temperature exceeds 1020°C; the latter at lower temperatures. CdS is found in the hexagonal form only. Experimental evidence indicates that a mixture of ionic and covalent bonding exists in (Zn;Cd)S, with estimates ranging from 22% to 75% ionic.

Band Gap: The band gap at room temperature is 3.70 ev and 3.64 ev respectively for the wurtzite and zincblende forms of ZnS. The gap for CdS is 2.43 ev. Since these values correspond to wavelengths of 3350A° and 3400A° for ZnS and 5100A° for CdS, ZnS crystals are transparent in the visible while CdS appears yellow because all wavelengths

less than 5100A^{o} are absorbed. As Cd is added to ZnS to form ZnCdS, the band gap decreases monotonically from 3.70 ev to 2.43 ev as a function of the percentage of Cd.

Preparation: These materials can be obtained as highly purified powders (from 1-50μ in grain size) and are then fired with the desired impurities. The cooled material (still in powder form) can then be deposited and experiments carried out. The production of crystals (usually 1mm in length or longer) is more complicated and the crystals grown show marked inhomogeneities in addition to being non-reproducible.

Impurities and Defects: The incorporation of impurities or defects causes new electron states to appear in the forbidden energy gap. These levels can be indirectly observed by a number of methods such as absorption bands, luminescence, and glow curves. The phosphors studied in this experiment are activated with group IB (Silver and Copper) substitutional impurities which replace Zinc or Cadmium.[2,3] This creates energy levels in the forbidden band above the top of the valence band. Group VIIB (Chlorine) and group IIIB (Aluminum) elements replace Sulfur and Zinc or Cadmium atoms respectively and enter as coactivators with energy levels lying in the forbidden band below the bottom of the conduction band.

In addition, Prenner and Williams[3] have proposed that these impurities are not uniformly distributed in the phosphor. An activator impurity and a coactivator impurity each constitutes locally an excess negative and positive charge, respectively, and therefore there is an electrostatic attraction between the two. At the firing temperatures of these phosphors where diffusion is rapid, this attraction leads to deviations from a random distribution of the two impurities. The activator and coactivator tend to be close together and form a pair whose interaction depends upon their separation.

Electrical conductivity can result from excitation of electrons and holes from discrete levels to the conduction and valence bands respectively. Electrons excited to the conduction band from the valence band and the holes remaining behind also contribute to conductivity. Hall Effect measurements[4] made over a wide range of exciting intensities on (Zn;Cd)S crystals of similar chemical composition to the phosphors used in this experiment show that the charge carriers are predominantly electrons.

B. Models Describing Luminescence and Photoconductivity in (Zn;Cd)S

Various phenomenological models have been proposed to explain luminescence and photoconductivity effects.

Essentially, a model is developed by postulating a set of discrete energy levels within the forbidden band and prescribing the allowed transitions. The solution of kinetic equations governing the time rate of change of electron or hole density in a band or at a discrete level leads to predictions of photoconductive and luminescent behavior.

A kinetic equation pertaining to a selected energy level is made up of charge carrier transition rate terms between the selected level and other levels allowed by the model. Five such terms are illustrated in Figure 1. They are: (1) interband excitation, proportional to the intensity of excitation; (2) thermal excitation of a charge carrier from a discrete level to a band, proportional to the product of a Boltzmann term and trapped carrier density; (3) excitation from a discrete level to a band, proportional to the density of occupied discrete levels and the intensity of incident exciting radiation; (4) recombination (and trapping) from a band to a discrete level, proportional to the product of free carrier density and unoccupied discrete level density; (5a) interlevel excitations proportional to the intensity of exciting radiation, the density of occupied acceptor levels and the density of unoccupied donor levels and (5b) recombinations proportional to the density of occupied donors and the density

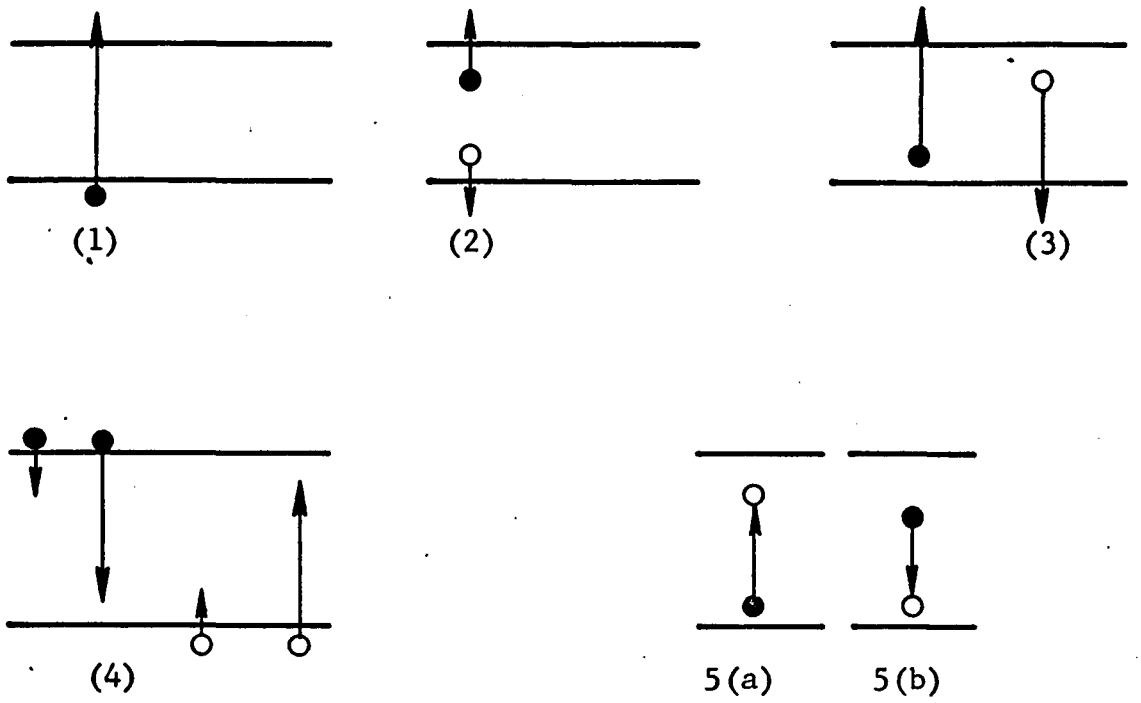

Figure I-1: Charge Carrier Transitions:

(1) Interband excitation; (2) thermal excitation; (3) excitation to a band from a discrete level; (4) recombination (and trapping) from a band to a discrete level; (5a) interlevel excitations and (5b) recombinators. Electrons are represented as dots and holes as circles.

of empty acceptors.

Schon[5] and Klasens[6] proposed a hole migration model for sulphides activated with monovalent impurities such as Cu or Ag to explain thermal and infrared quenching of luminescence. Figure 1-2a illustrates this model for the case where interband (fundamental absorption) excitation takes place. Absorbed light excites a free electron to the conduction band and leaving a hole in the valence band. Both charge carriers contribute to the conductivity. The hole migrates toward an occupied activator center and is captured there, giving of a small amount of energy as infrared radiation or as vibrational quanta. The electron wanders through the lattice and finally comes near the unoccupied activator center where it is captured, giving off energy as luminescent emission. Schon and Klasens found it necessary to modify the model described above by introducing a set of electron trap levels below the conduction band which are not connected to the activators. The additional existence of very shallow traps (or equivalently, excited activator centers) lying just below the conduction band has been suggested.[7,8] Luminescent recombination transitions could then take place without requiring electrons to recombine directly by route of the conduction band. Nonluminescent transitions (quenching) would be explained by the recombina-

Figure I-2a: The Schon-Klasens Model for Sulfides with Monovalent Activator: (1) excitation; (2) hole migration; (3) hole capture(nonradiative); (4) electron migration; (5) electron capture resulting in luminescence.

Figure I-2b: The Lamb-Klick Model for Sulfides with Monovalent Activator: (1) excitation; (2) hole migration; (3) radiative hole capture (4) electron migration; (5) electron capture(nonradiative).

Figure I-2c: The Prener-Williams Model for Sulfides: (1) excitation; (2) and (3) thermal inter and intra-state donor-band transitions; and (4) recombination.

Models for Sulfides

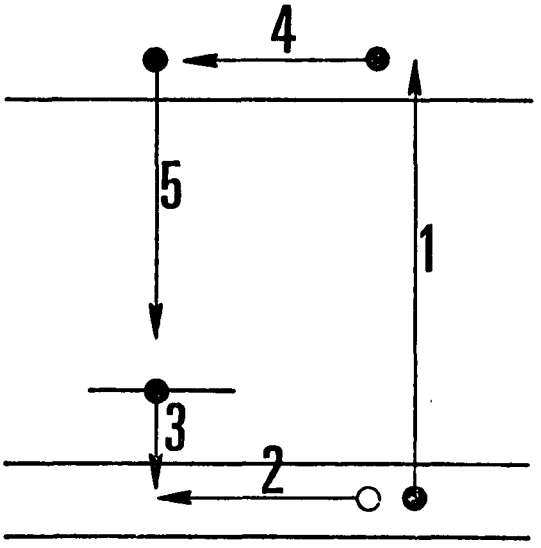

Figure I-2a

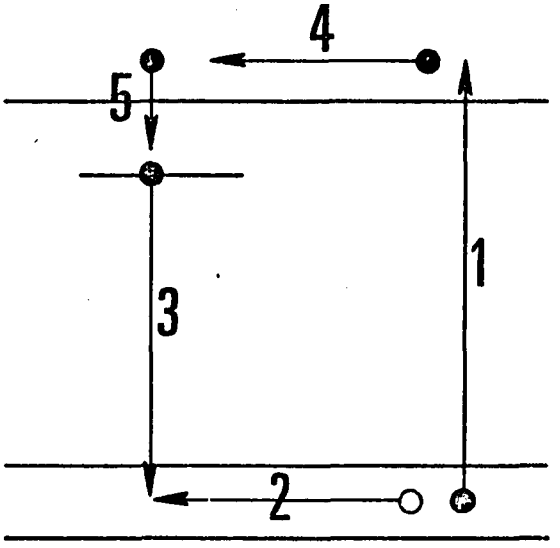

Figure I-2b

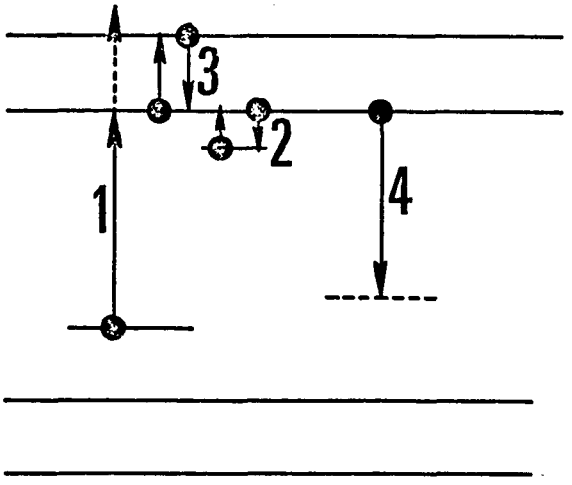

Figure I-2c

tion of free or trapped electrons with holes produced thermally or by infrared.

The model of Lamb and Klick[9] is illustrated in Figure 1-2b. It differs basically from the Schon-Klasens model in that the capture of a free hole in the valence band by a trapped electron results in luminescence. Free electron capture is associated with luminescence in the Schon-Klasens model. Lamb and Klick proposed their model to explain the difference in decay times of luminescence and photoconductivity.

In the Prenner and Williams[3] model transitions are allowed between relatively close lying (associated donor-acceptor pairs) discussed above. Figure 1-2c is illustrative of this model. Light is absorbed (1), causing an electronic transition from the ground state of the acceptor to either the donor state or to the conduction band. Transitions (2), between excited and ground donor states are allowed as well as transitions (3), between donor states and the conduction band. The ground state is assumed to be the trapping state. The unoccupied acceptor state is assumed to be perturbed upward due to atomic rearrangement within the lattice. The luminescent transitions (4), are between the excited donor state and the perturbed acceptor state. The excited donor states are chosen because they

have large orbits and therefore may overlap the lowlying state associated with the acceptor thus facilitating transitions between the two. One consequence of this model is that the luminescent transition is essentially independent of the donor (coactivator) present since the excited state of all donors is considered to be near the band edge.

Shionoya et al[10] introduced the concept of a two-level unassociated pair model. The pairs are termed unassociated in that the substituted impurities are assumed to be uniformly distributed in the phosphor. The Shionoya model was used to explain the variation of the luminescent spectrum with intensity of incident exciting radiation as well as the shift in the maxima of the luminescent spectrum during decay. High concentrations of impurities, resulting in closer spatial separation between donors and acceptors, suggests associative pairing while smaller impurity concentrations lead to behavior better explained by unassociative pairing.

The diverse models listed above, each of which may explain measured physical phenomena in terms of different mechanisms governing electronic transitions, illustrate the fact that electronic processes in the sulfides are not completely understood as of this date.

C. Measurement of Photoconductivity with D.C. and A.C. Methods

Measurements of photoconductivity of ZnS and CdS phosphors have been made on powder and single crystal specimens.[11,12] The study of each form of the phosphor offers advantages and disadvantages. Diffusion of exciting radiation and emitted light due to the inherent particulate nature of powders does not occur with crystals. Isotropic properties, such as preferred directions of current flow and polarization of luminescent output, can be studied only in crystals. However, crystal inhomogeneities, which are commonly observed,[13] would misrepresent the inherent phosphor characteristics. A region of high resistance, for example, would lead to a completely incorrect experimental determination of conductivity. Also, crystals cannot be exactly replicated. Phosphor powder samples tend to average out localized inhomogeneities found in crystals. Various powder samples may be made from the same preparation and therefore comparisons between results of experiments performed on different samples are consistent.

The earliest measurements of conductivity were made on phosphor powders with D.C. techniques.[14,15,16] The samples were prepared by sandwiching the phosphor powder between metal plates or glass plates with a transparent

conducting surface layer. Later, similar measurements[17, 18,19] were made on single ZnS and CdS crystals. The crystal samples were prepared by using metal paste electrodes or evaporation of films on the surface of the crystal. It was found[7] for powders that a nonohmic relationship between the induced current and the applied field existed at all fields, except when the highest field strengths (10,000 volts/meter) were used. The presence of inter-grain barrier potentials and contact potentials between the electrodes and the surface of the powder were suggested[20] as the cause of the nonohmic behavior of the powder. Similar experiments[12] performed with single crystals showed an ohmic relationship, which supports the idea of grain surface barrier effects. Measurements made with crystals, however, could be of limited value due to contact potentials which cannot be easily corrected.

The presence of surface effects on conductivity was deduced[18] by noting changes in photoconductivity for the same crystal under tests in air and in vacuum. It was found that the photosensitivity of CdS and ZnS crystals increased by changing from an air to a vacuum environment. Voyatzaleis[21] found the opposite to be true for sulfide powders.

A.C. investigative techniques have been used on CdS

crystals[9,22] and CdS and ZnS powders[23,24,25] in order to minimize electrode and surface barrier effects.

The apparent change in dielectric constant and conductance of ZnS powders was measured[24] in the frequency range of 0.1 to 10 megacycles. These measurements were interpreted on the basis that trapped electrons which were assumed to be capable of remaining trapped while moving distances over 1000 times interatomic spacing are responsible for the impedance changes observed.

Other[23,25] A.C. measurements on (Zn;Cd)S powders (made at the order of one kilohertz) indicated that these changes are due to the change in conduction electron density. It was postulated that the powder has to be considered as an inhomogeneous system where a high-resistive-layer represents the high-resistance grain boundaries and the air spaces between the phosphor grains. Another layer which is radiation sensitive represents the interior of the grains. This two-layer model was shown to be equivalent to two condensers in series, one of which is shunted by a radiation sensitive resistance. As the resistance decreases with increasing excitation, the effects of the capacitance associated with it becomes increasingly negligible, and finally only the capacitance of the nonconductive layer remains, resulting in a saturation value of the measured

capacitance. The measured capacitance of the phosphor sample was shown to be monotonically increasing with conductivity. A.C. measurements results thus interpreted were seen to be similar to the results of D.C. measurements on crystals thereby adding to the credibility of assumed high-resistance surface layers.

When insulating barriers were deliberately inserted between CdS crystals and the electrodes in a variation of the usual A.C. conductivity determination[25] it was found that results could not be explained in terms of the simple series combination of two capacitors with a photosensitive resistance shunting one. This is probably due to a nonuniform charge distribution in the crystal.

A theoretical calculation[26] has shown that the relatively low frequencies used in the experiments described above cause a nonuniform distribution of charge carriers which form a depletion layer on one side of the phosphor grain or crystal and an accumulation charge layer on the other.

As the external field drives free charges toward the grain boundaries (thus decreasing the densities of free charges in the interior), the originally trapped carriers evaporate into the conduction or valence band and are also swept toward the grain boundaries where they con-

tribute to the excess charge or are retrapped. The overall effect of the motion of the free and evaporated charge is to screen the interior of the phosphor grains causing an increase in the measured capacity of the phosphor sample. This measurement would then be interpreted to indicate a larger conductivity than is actually the case. Recent measurements[27] seem to corroborate this calculation.

D. Measurement of Photoconductivity at Microwave Frequencies

The innovative part of this experiment is the use of a microwave bridge circuit to measure the propagation constant of the electromagnetic wave in the phosphor powder. The propagation constant is then related to the photoconductivity. Other microwave techniques have been used in the investigation of the recombination rate and lifetime of photocarriers in Ge and Si[28,29] and photoconductive modulation in CdS.[30] Shepard[31] has used sensitized CdS powder with a beam of light to attenuate microwave signals. Dziesiaty[32] made qualitative determinations of the photoconductive excitation spectrum and light characteristics in CdS and CdSe single crystals.

This experiment makes use of a microwave bridge to make quantitative measurements of the photoconductivity of activated CdS and ZnS phosphor powders. The photoconduc-

tivity is determined by a waveguide perturbation calculation of the wave propagation characteristics in the phosphors. The inherent advantages of this type of measurement are many. Electrodes are not needed and therefore the problem of contact potentials does not arise. At high microwave frequencies (10 gigahertz) intergrain potential barriers are not important. A simple computation shows that free electrons are displaced approximately 10 angstroms during a half cycle of the applied field. Since the powder grains are larger than several microns, grain polarization and evaporation of trapped charge is not likely to occur at these frequencies. Therefore the charge density at the interior of the grains remains unchanged. Thus, measurements made at microwave frequencies presumably do not disrupt the phenomena being investigated.

E. Summary of Results

The experimental results, all at room temperature, will be described in three parts. The first will deal with the determination of the conductivity vs light intensity relationship and the calculation of the corresponding electron densities. The second will treat the effects obtained with simultaneous application of ultraviolet and infrared radiation after equilibrium is reached. The last

part will report on measurements of the rise and decay of luminescence and conductivity due to UV excitation.

An overall view of the results found in this investigation are:

1. The photoconductivity of ZnS phosphors activated with Cu and Cl or Cu and Al (green emission) shows a very weak dependence on the exciting intensity. Using the relationship $\sigma \propto I^n$, n is found to vary between 0.23 and 0.36 over a wide range of exciting intensities.

2. For all phosphors measured, the infrared quenching of the photoconductivity is equal to or greater than the quenching of the luminescence.

3. Rise and decay times of the photoconductivity are considerably greater than corresponding times for the luminescence.

It is shown that these results are in disagreement with the Schon-Klasens model, but can be explained if this model is revised to take into account the fact that a range of luminescent centers exists having varying transition probabilities.

II. Apparatus and Experimental Techniques

A. Description of Apparatus

1. Microwave Bridge

The basic component of the experimental setup is a microwave bridge[32,33] which is used to determine the photoconductivity of the phosphor. A block diagram of the bridge appears in Figure II-1. It is composed of a generator arm, two collinear arms, a detector arm and magic (hybrid) tee, which is a junction common to all arms.

The phosphor sample is introduced in the bridge in one of the collinear arms. An enclosure, built around the waveguide section housing the phosphor sample, permits optical excitation and detection of the luminescent output of the phosphor.

The klystron generates a continuous wave signal of 10.5 gigahertz at power levels between 200 and 500 mW. It is frequency-locked to a harmonic of a standard crystal incorporated in the frequency stabilizer and its power output is monitored by a power meter. A resonant cavity frequency meter determines the frequency.

The relevant components of arm (1) are a variable precision short and a precision attenuator, and those of arm (2) are one precision attenuator, the sample holder

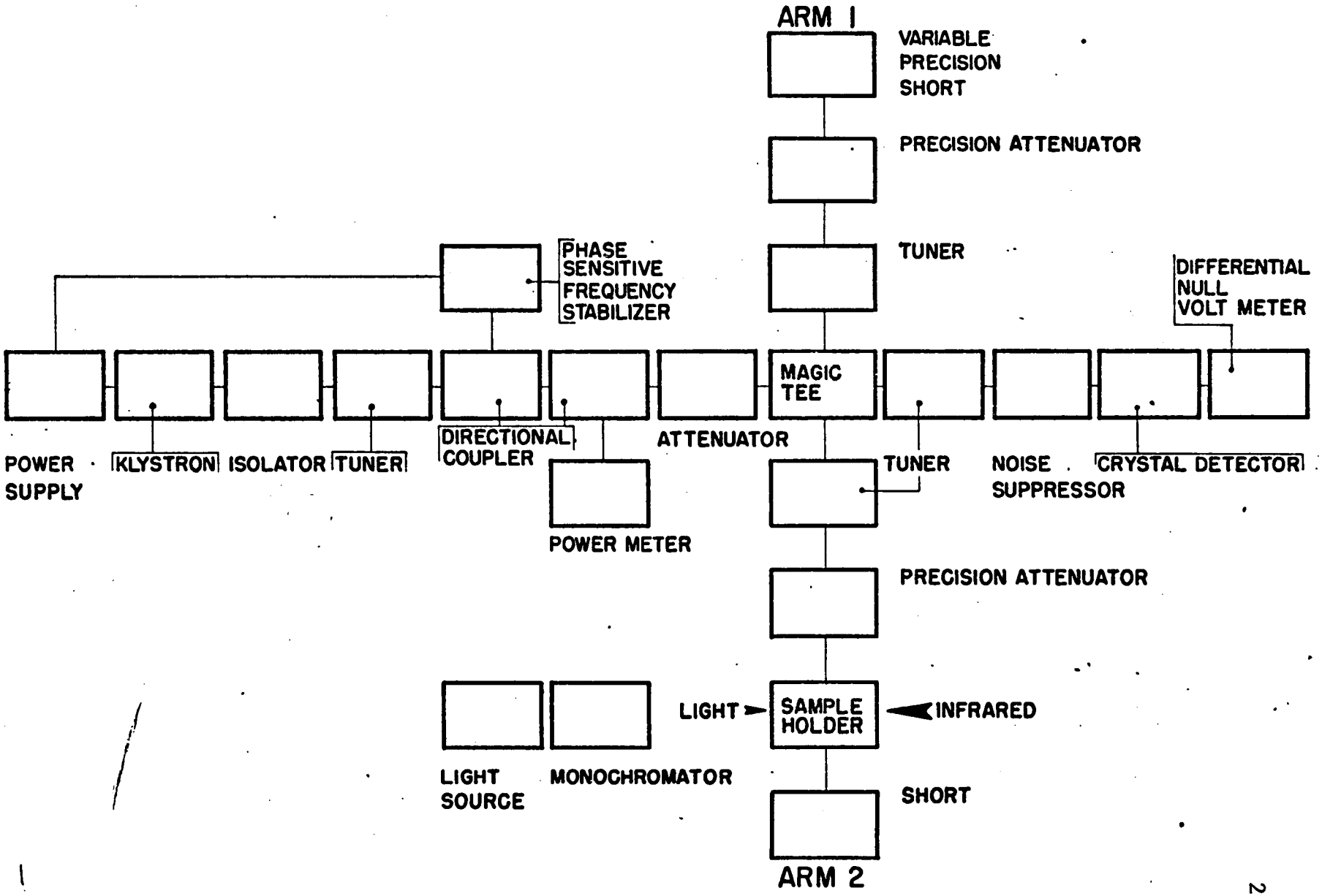

Figure II-1: The Microwave Bridge

assembly, and a variable short. Equal lengths of the collinear arms insure that the bridge circuit is minimally effected by an overall change in temperature of the system. A simple calculation shows that a two degree centigrade change in temperature would generate a 25% error in conductivity if the collinear arms differed in length by ten inches.

The detector arm consists a tuner, an attenuator, a noise suppressor, and a detector mount for a diode crystal. The diode is a square law detector in that its response is proportional to the square of the amplitude of the incident electric field.

2. Sample Holder Assembly and Light Entry and Detection System

The samples were made by depositing a thin layer of phosphor powder (about 0.01 cm thick, 3.5 cm x 2.2 cm) between two sheets of glass, each 0.025 cm thick. A small amount of Duco cement was used as a binder for the phosphor powder. The sample was slanted at both ends to eliminate[34] microwave reflections at the two air-sample interfaces. The surface density of the phosphor samples ranged between 5 and 35 mg/cm^2. Figure II-2 shows a phosphor sample mounted in the sample holder assembly.

A section of rectangular X-band waveguide was modi-

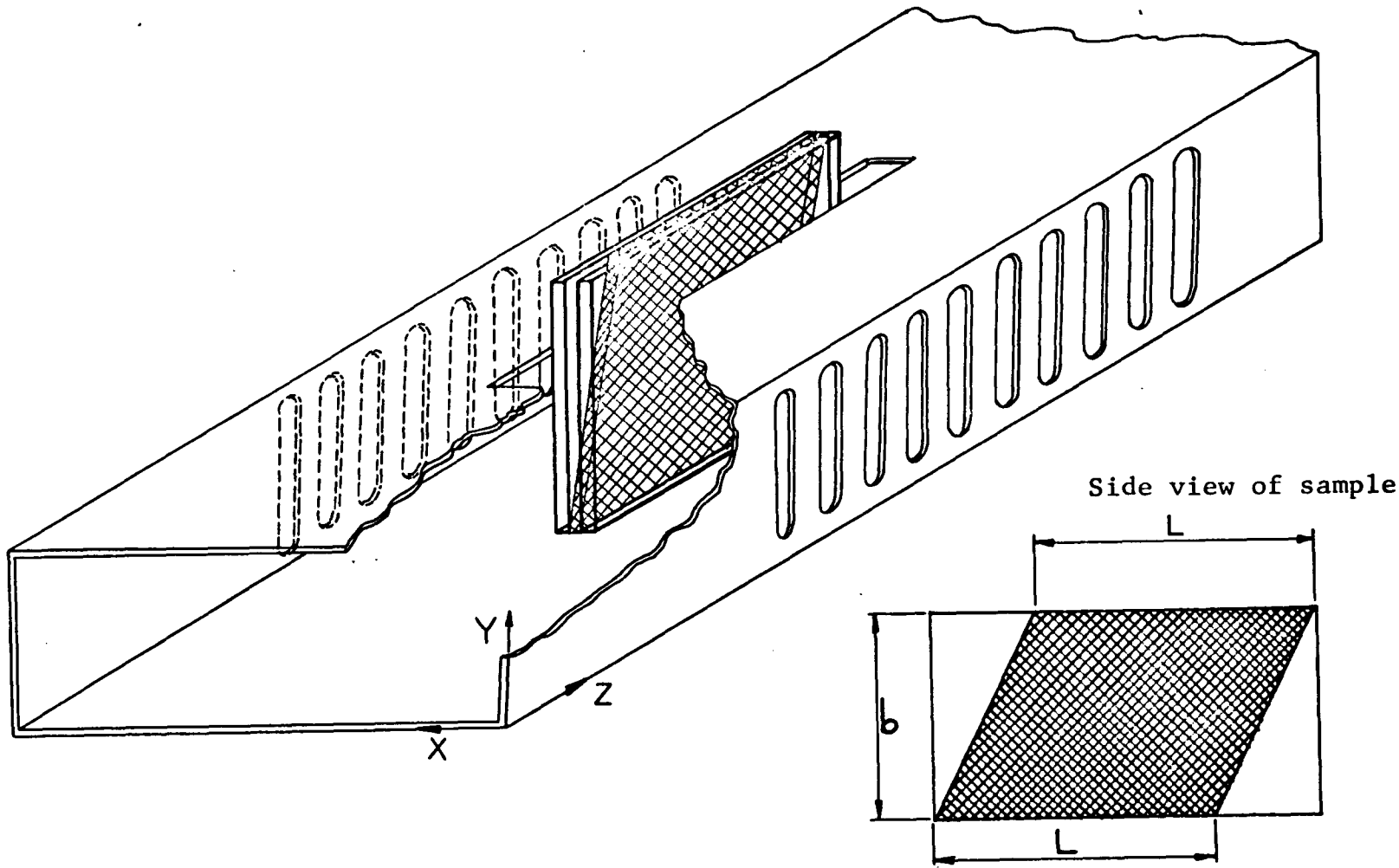

Figure II-2: Phosphor Mounted in Phosphor Holder Assembly.
Note: The sample (cross-hatched) is between the two glass plates (clear).

fied to serve as the sample holder assembly. A thin (0.12 cm) slot, 5 cm long was cut along the center of the wide waveguide wall. The sample was inserted into the interior of the waveguide section through this slot. Narrow (½ mm) uniformly spaced (½ mm apart) slots cut along both narrow walls of the guide served as entrance apertures for light. Microwave radiation losses were small since all slots run along current lines.

The light entry and detection system is shown in Figure II-3. The sample holder assembly was enclosed in a light-tight rectangular sheet metal box. Hollow cylindrical piping (portals (1) and (2)) was attached to the sheet-metal faces directly opposite the slotted narrow waveguide walls. A filter housing a shutter mechanism was built onto the metal piping. The sample could thus be simultaneously illuminated by two light beams.

Ultraviolet light entered through portal 2. The ultraviolet source was a high pressure Xenon 90K-1 150 watt lamp. Excitation spectra were obtained with the use of Bausch and Lomb grating monochrometer (3500Å to 8000Å), a narrow band Corning 7-83 filter (centered at 3650Å) and a broad band Corning 4-96 filter (3600Å to 6000Å). Wratten neutral density filters ND1, ND2, and a combination of wire meshes were employed to reduce the ultraviolet excitation

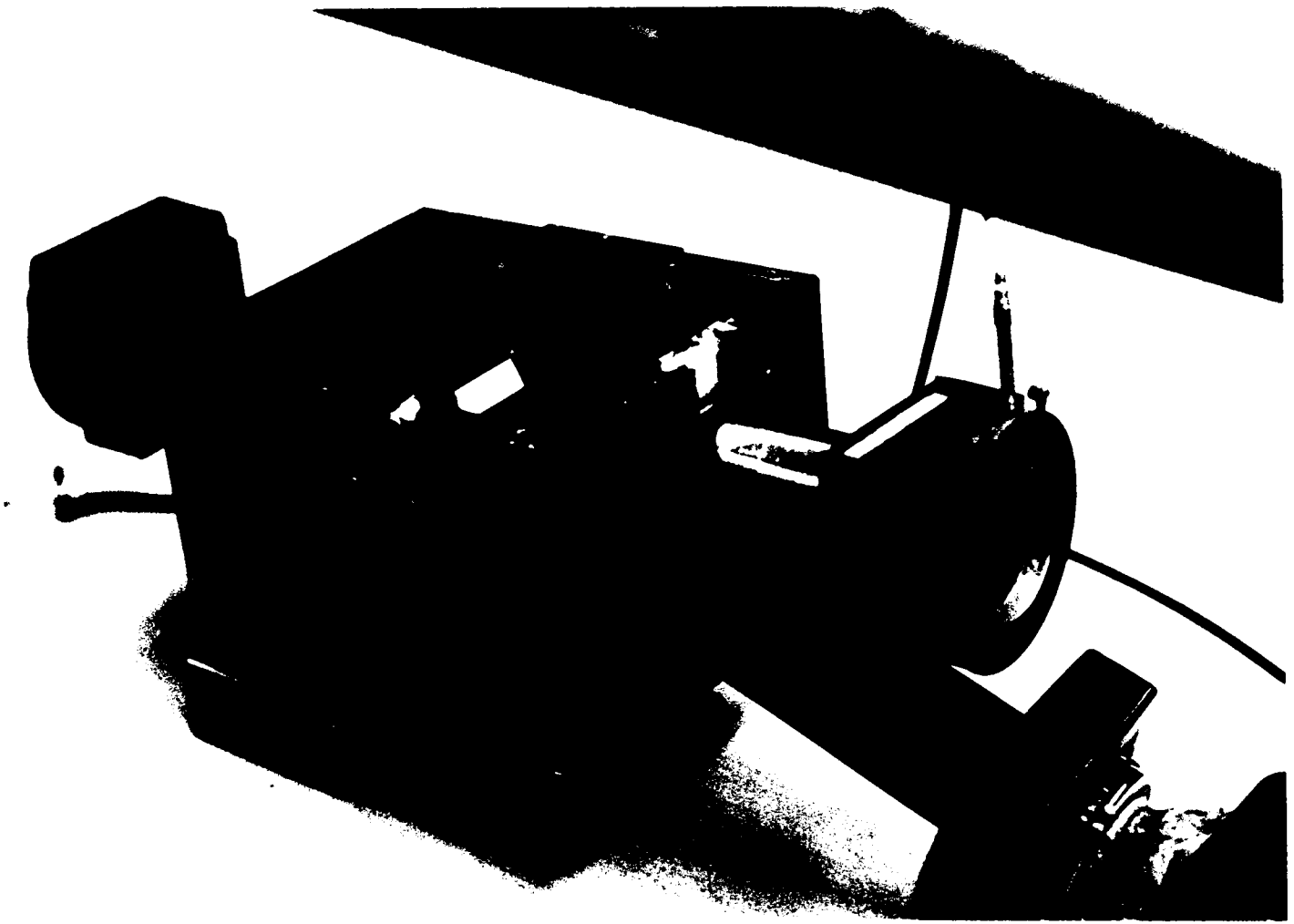

Figure II-3: Light Entry and Detector System.

by known amounts as determined by an Eppley thermopile.

Portal 1 served as an entry for the infrared beam. The infrared light source was a 750 W slide projector used with a Bausch & Lomb monochrometer (7000Å to 16000Å) or a suitable filter and water cell combination. Near infrared radiation, between 7000Å and 10000Å, was obtained by using two Corning 7-69 filters and a 25 cm long water cell. The infrared intensity was controlled by varying the voltage of the source. The transmission spectra of this source is shown in Figure II-4. It was obtained from water spectral attenuation data[35] and the Corning filter catalogue. The intensity was also calibrated with the Eppley thermopile.

Portal 3 was constructed similarly to portals 1 and 2. It is directly below portal 2, jutting out at an angle of about 30 degrees with the normal to the sheet metal face. A housing, which contained an RCA 1P21 photomultiplier tube, was attached at the termination of portal 3. The photomultiplier output was monitored by a microammeter to which was attached a recorder.

Only a narrow band of the luminescent spectrum was allowed to pass through the photomultiplier. A Corning 4-105 filter (centered at 5150Å) was used as a band-pass filter for phosphors luminescing primarily in the green. A Corning 5-74 (centered at 4330Å) filter was the band-pass

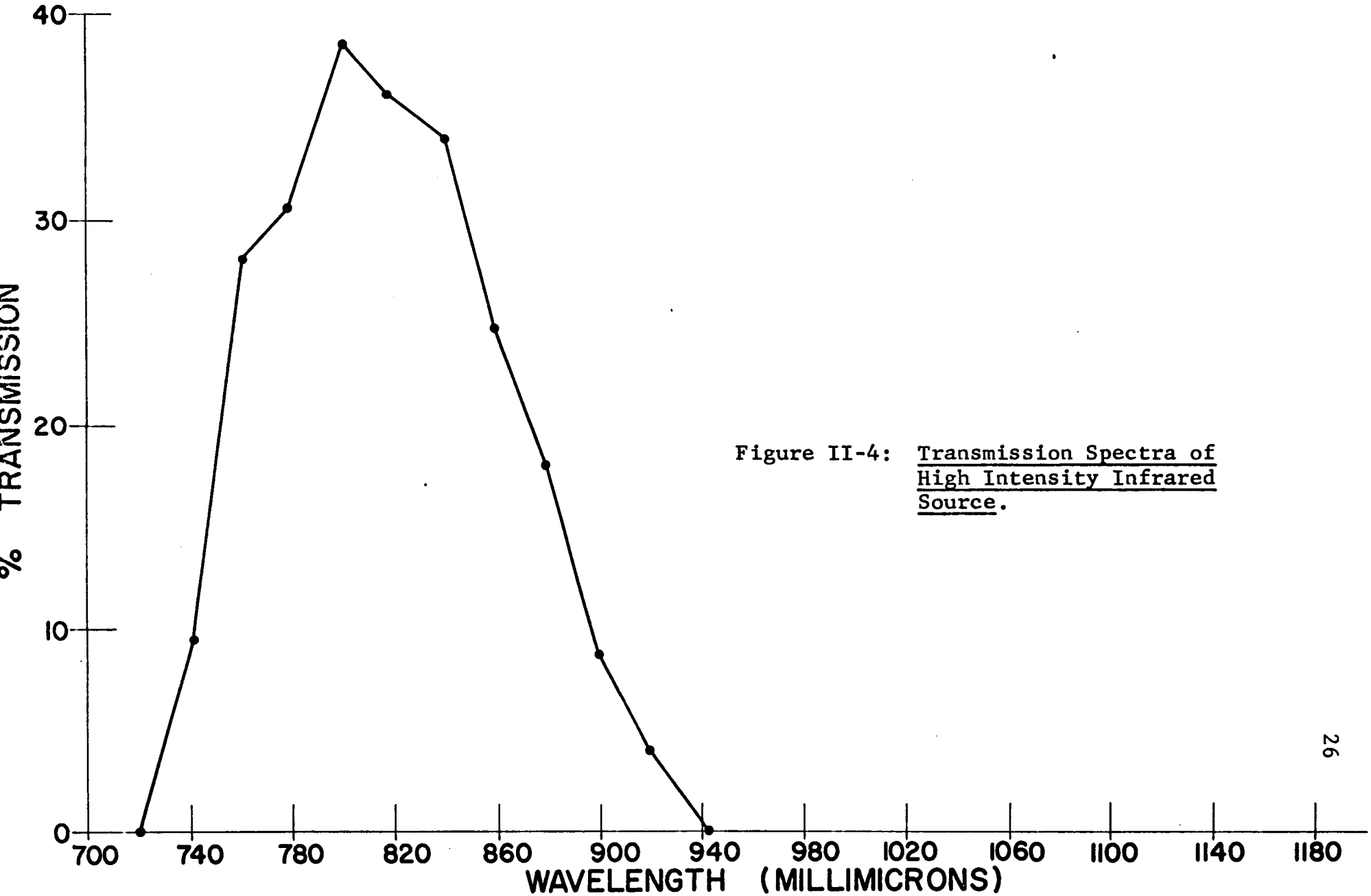

Figure II-4: Transmission Spectra of High Intensity Infrared Source.

filter used for phosphors luminescing primarily in the blue.

B. Operational Use of Microwave Bridge

1. Power Absorbed by Detector

The dimensions of the waveguide and the operating range of the klystron allow only the dominant TE_{10} mode to be propagated in the guide. The criteria for neglecting higher order modes in the sample and its immediate vicinity are satisfied (Appendix A). Therefore only the TE_{10} mode is considered in this calculation.

In the empty guide the electric field is given by[36]

$$E_y(x,z,t) = A \sin \frac{\pi x}{a} e^{-\gamma_0 z + j\omega t}$$

$$E_x = E_z = 0$$

where

$$\gamma_0 = \alpha_0 + j\beta_0$$

The magnetic field is given by II-1

$$H_z(x,z,t) = \frac{jA\pi}{a\omega\mu_0} \cos \frac{\pi x}{a} e^{-\gamma_0 z + j\omega t}$$

$$H_x(x,z,t) = \frac{j\gamma_0 A}{\mu_0 \omega} \sin \frac{\pi x}{a} e^{-\gamma_0 z + j\omega t}$$

where a is the width of the broad waveguide wall, γ_0 the propagation constant in the empty guide, α_0 and β_0 the attenuation and phase constants respectively in the empty guide, A the amplitude of the electric field, μ_0 the permeability of free space, ω the angular frequency of the

guide signal, and $\hat{z}$ is the direction of propagation. Figure II-2 shows the coordinate system.

The (space dependent part of the) signal at the matched detector which passed through collinear arm (1) is given by (origin taken at the magic tee)

$$E_{1D} = \frac{E_0}{\sqrt{2}} \sin \frac{\pi x}{a} \; e^{-(\alpha_0 + j\beta_0) 2 S_1} \qquad \text{II-2}$$

where E_0 is the electric field is the generator arm and S_1 is the length of arm (1). The factor 2 appears in (II-2) because the klystron power is split evenly at the magic tee.

The signal at the detector which passed through arm (2) containing the sample is given by

$$E_{2D} = \frac{E_0}{\sqrt{2}} \sin \frac{\pi x}{a} \; e^{-(\alpha_0 + j\beta_0) 2 (S_2 - L)} \; e^{-(\alpha_D + j\beta_D) 2L} \qquad \text{II-3}$$

where L is the length of the phosphor sample, S_2 is the length of collinear arm (2), α_D and β_D are the effective attenuation and phase constants of the nonilluminated phosphor. The factor 2 appears in the exponent of (II-2) and (II-3) because the signal passes twice through the collinear arms and the phosphor.

Balance is achieved by adjusting the precision short and precision attenuator in arm (1) so that the signal at the detector is zero. The signal received at the detector

when balance obtains is

$$\Delta E_D = E_{2D} - E_{1D} = 0$$

The minus sign appears in the above because the signal in the detector arm, due to the characteristics of the magic tee, is proportional to the difference in signals in the collinear arms. When the phosphor is illuminated, the bridge is unbalanced and the signal at the detector becomes

$$\Delta E = E_2 - E_{1D} = E_2 - E_{2D}. \qquad \text{II-4}$$

E_2 is the signal (at the detector) which passes through the illuminated phosphor and is given by

$$E_2 = \frac{E_0}{\sqrt{2}} \sin\frac{\pi x}{a}\, e^{-(\alpha_0 + j\beta_0)2(S_2 - L)}\, e^{-[(\alpha_D + \Delta\alpha) + j(\beta_0 + \Delta\beta)]2L} \qquad \text{II-5}$$

where $\Delta\alpha$ and $\Delta\beta$ are the changes in the effective attenuation constant and effective phase constant of the phosphor due to illumination.

The average power absorbed by the matched detector is given by[36]

$$\Delta P = \frac{1}{2} \int_{x=0}^{a} dx \int_{y=0}^{b} \mathrm{Re}\, \Delta\vec{E} \times \Delta\vec{H}^{*}\, dy \qquad \text{II-6}$$

which reduces to

$$\Delta P = K_p \left(1 + e^{-4\Delta\alpha L}\left(1 - 2\cos 2\Delta\beta L\right)\right) \qquad \text{II-7}$$

where

$$K_p = \frac{1}{8}\frac{\beta_0 E_0^2}{\omega\mu_0}\, ab\, e^{-4\alpha_0(S_2 - L)}\, e^{-4\alpha_0 L} \qquad \text{II-8}$$

If $|2\Delta\alpha| \ll 1$ and $|2\Delta\beta L| \ll 1$ then (II-7) becomes

$$\Delta P = K_p \left[(2\Delta\alpha L)^2 + (2\Delta\beta L)^2\right] \qquad \text{II-9}$$

Only terms up to second order have been retained. Equation (II-9) shows that the power absorbed by the matched detector is proportional to two independent quadratic terms: the attenuation and phase shift change due to illumination of the phosphor.

2. Correlation of Attenuation and Phase Change to Measured Quantities

Attenuation or insertion loss as measured in decibels, h , for a component is in waveguide circuit is given by

$$h = 10 \log_{10} \frac{P_1}{P_2} \quad (db) \qquad \text{II-10}$$

where P_1 is the power incident on, and P_2 is the power transmitted by the waveguide component. Let the electric field at the leading edge of the phosphor be given by E and then the electric field at the termination of the phosphor is given by $E\, e^{-(\alpha_0 + j\beta_0)L}$. Since power is

proportional to the electric field squared, the attenuation due to the insertion of the phosphor sample in the waveguide interior is

$$h = 10 \log_{10} \frac{|E|^2}{|E|^2 e^{-2\alpha_p L}} \quad (db) \qquad \text{II-11}$$

$$= 8.68 \alpha_p L$$

The change in attenuation, Δh, resulting from the change in the attenuation constant, $\Delta \alpha$, when the sample is illuminated is from (II-11)

$$\Delta h = 8.68 \, \Delta \alpha \, L \quad (db) \qquad \text{II-12}$$

The precision attenuators in arms (1) and (2) are calibrated directly in db. The insertion loss, h , was found experimentally by inserting the phosphor sample in the bridge circuit and balancing the bridge by adjusting the precision attenuator in arm (2) until a minimum signal was registered by the detector. The change in setting of the precision attenuator is the insertion loss.

In order to determine the phase constant β_p of the phosphor, it is necessary to consider the adjustments which rebalance the bridge circuit in phase after the phosphor is inserted into the waveguide interior. Initially, with the phosphor sample outside of the guide, the bridge is balanced. Then the phosphor sample is inserted into the waveguide interior and the microwave bridge is rebalanced

in phase by adjustment of the precision short at the end of arm (1). The change in phase of the signal passing through arm (2), $\Delta\theta_2$, is given by

$$\Delta\theta_2 = \left[\frac{2\pi}{\lambda_0} 2(S_2-l) + \frac{2\pi}{\lambda_D} 2L\right] - \frac{2\pi}{\lambda_0} 2S_2$$

$$= \left(\frac{2\pi}{\lambda_D} - \frac{2\pi}{\lambda_0}\right) 2L$$

where λ_0 is the signal wavelength in the empty guide and λ_D is the effective wavelength of the microwave signal in the phosphor. Similarly, one has for the phase change, $\Delta\theta_1$ of the signal passing through arm (1)

$$\Delta\theta_1 = \frac{2\pi}{\lambda_0}(2S_1 + 2x) - \frac{2\pi}{\lambda_0} 2S_1$$

$$= \frac{2\pi}{\lambda_0} 2x$$

where x is the change in the distance setting of the precision short. Since adjustment to a minimum signal is equivalent to equal phase change in both arms, we have

$$\frac{2\pi}{\lambda_0} x = \frac{2\pi}{\lambda_D} L - \frac{2\pi}{\lambda_0} L \qquad \text{II-13}$$

Identifying the phase constant in the empty guide as $\beta_0 = \frac{2\pi}{\lambda_0}$ and the phase constant in the phosphor obstacle as $\beta_D = \frac{2\pi}{\lambda_D}$, the above may be written as

$$\beta_D = \left(\frac{x}{L} + 1\right)\beta_0 \qquad \text{II-14}$$

When the sample is illuminated, the change in phase constant, $\Delta\beta$ is from (II-14)

$$\Delta\beta = \frac{\Delta x}{L}\beta_0 \qquad \text{II-15}$$

where Δx is an additional change in the setting of the precision short. β_0 is determined by measuring the signal

frequency.

3. Detector Circuit

The detector used in these experiments is an IN 23B crystal diode. The diode was placed in series with a 30K ohm resistor, and the potential across the entire resistor was measured by a D.C. differential null voltmeter. The output from the voltmeter was fed to a recorder. The detector response, V , is proportional to the power absorbed by the crystal. For a matched detector, one has from (II-9)

$$V = K_c \Delta P = 4 K_c K_p \left[(2\Delta\alpha L)^2 + (2\Delta\beta L)^2 \right] \qquad \text{II-16}$$

where K_c is a constant depending on the crystal used. Substituting (II-12) and (II-15) into (II-16) one has,

$$V = 4 K_c K_p \left[\left(\frac{\Delta h}{8.68}\right)^2 + (\beta_0 \Delta x)^2 \right] \qquad \text{II-17}$$

Equation (II-17) was tested as follows. The bridge was balanced and then Δh was varied keeping Δx fixed. The ratio $\left(\frac{\Delta h}{V}\right)^2$ was calculated, and was found to be constant ($\pm$ 5%). Similarly, Δx was varied holding Δh fixed and the ratio $\left(\frac{\Delta x}{V}\right)^2$ was also constant ($\pm$ 5%).

4. Relation of Photoconductivity to Attenuation and Phase Measurements

The conductivity is given by[37]

$$\sigma_r - j\sigma_i = \frac{N e^2 \tau}{m} \left(\frac{1 - j\omega\tau}{1 + \omega^2\tau^2} \right) \qquad \text{II-18}$$

where σ_r and σ_i are the real and imaginary parts of the conductivity related by $\sigma_i = \omega\tau\sigma_r$. N is the free electron density, τ the time between scattering collisions and m and e are the effective electron mass and charge respectively.

A perturbation calculation given in Appendix A which makes use of Equations (II-18), Maxwell's equations and the defining equations for complex permittivity, $\epsilon = \epsilon_0(\kappa_r + j\kappa_i)$ (where $\epsilon_0\kappa_i$ is due only to dielectric loss), results in two expressions which relate the propagation characteristics of the microwave signal to the conductivity and permittivity of the sample. The results are the following:

$$\mu_0\omega t(\sigma_r + \omega\epsilon_0 k_{pi}) + 2\mu_0\omega^2\epsilon_0 k_{gi} t_g = a\alpha_0\beta_0 \qquad \text{II-19}$$

(the 2 appears because there are two glass plates) and

$$\frac{a}{2}\left[\beta_0^2 - \alpha_0^2 - \beta_0^2\right] = \mu_0\omega^2\epsilon_0\left[(k_{gr}-1)2t_g + (k_{pr}-1)t - \frac{\tilde{\Gamma}}{\epsilon_0}\sigma_r t\right] \qquad \text{II-20}$$

where k_{pr} and k_{pe}, k_{gr} and k_{ge}, are the real and imaginary parts of the permittivity, respectively of the phosphor and glass. t and t_g are the thicknesses of the phosphor and glass surfaces, respectively, a is the thickness of the short waveguide wall and L is the length of the phosphor sample.

Photoconductivity is the increase in the electrical conductivity of a material (insulator and semiconductor) caused by incident radiation. The direct effect is to

increase the number of mobile, or free, carriers in the material. Thus, when radiation impinges upon the sample, there is an additional small loss, $\Delta\alpha$, and small phase shift, $\Delta\beta$, due to the increase in conductivity (Experimental results show that $\left(\frac{\Delta\alpha}{\alpha_D}\right), \left(\frac{\Delta\beta}{\beta_D}\right) << 1$). Since only a very small percentage of the atoms in these phosphors are activators (impurities) and only a very small fraction of activators are ionized at any time it is assumed that both the real and imaginary parts of the permittivity remain constant. If the change in conductivity of the phosphor is small, then it may be related to the change in propagation constants by taking incremental changes of Equations (II-19) and (II-20) and neglecting second-order terms. Results are

$$\Delta\sigma_r = \frac{q}{\mu_0 \omega t} \left\{ \alpha_D \Delta\beta + \beta_D \Delta\alpha \right\} \qquad \text{II-21}$$

and

$$\Delta\sigma_r = \frac{q}{\mu_0 \omega^2 \tau t} \left\{ \alpha_D \Delta\alpha - \beta_D \Delta\beta \right\} \qquad \text{II-22}$$

Equation (II-2) expressed in terms of experimental observables becomes with (II-11) thru (II-15),

$$\Delta\sigma_r = \frac{q}{\mu_0 \omega t} \frac{2\pi}{8.68\lambda_0} \frac{1}{L^2} \left(h\Delta x + (x+L)\Delta h \right) \qquad \text{II-23}$$

and is the equation used to determine the conductivity change.

The preceding analysis assumed uniform exciting in-

tensity throughout the phosphor sample. Appendix B shows how the photoconductivity can be calculated for the case of nonuniform excitation.

Using Equations (II-21) and (II-22), the experimental value of τ was found to be roughly 10^{-13} sec. This agrees with the literature.[37] Since $\omega\tau \simeq 6\times10^{-3}$, it is seen from Equation (II-18), that $\sigma_r = \frac{Ne^2\tau}{m}$, which is the D.C. conductivity.

5. Balanced Bridge Method for the Determination of Conductivity

A dark, unexcited phosphor sample was inserted into the sample holder assembly when the bridge was at balance. The bridge was then rebalanced by increasing the attenuation in arm (1) by h (db) and adjusting the precision short located at the end of arm (1). The phosphor sample was then irradiated with ultraviolet light which again brought the microwave bridge to a state of imbalance. The bridge was then rebalanced through additional changes in attenuation, Δh , and path length, Δx . The experimental data were used to determine the conductivity from Equation (II-21). The results showed that $(x+L)\Delta h \gg h\Delta x$ held for all measured cases. This indicates that the increased carrier density is due mainly to the additional attenuation of the microwave signal.

6. Unbalanced Bridge Method for the Determination of Photoconductivity

When the unexcited phosphor is illuminated with weak ultraviolet light ($1\ \mu$ watt/cm^2), the experimental value of Δh is of the order of 0.001 db. The null method is not suitable for measurements at these ultraviolet intensity levels since the most precise low scale range of the (rotary vane) precision attenuator used in the experiment has an uncertainty which is also of the order of 0.001 db. Small changes of attenuation in collinear arm, however, effect an appreciable signal change at the detector if the bridge is initially unbalanced. The development which follows shows how the change of signal at the detector for an unbalanced bridge is related to the change in conductivity of the phosphor.

Reference is made to Equations (II-16) which may be rewritten as

$$V = K_o \left[(\Delta\alpha)^2 + (\Delta\beta)^2 \right] \qquad \text{II-24}$$

where K_o is an overall constant. For the purpose of this derivation it is convenient to rename the detector response in terms of new symbols

$$V_c = K_o \left[(\delta\alpha)^2 + (\delta\beta)^2 \right] \qquad \text{II-25}$$

where $\delta\alpha$ is an arbitrary attenuation decrease effected in arm (1) by adjusting the precision attenuator and $\delta\beta$ is an arbitrary phase increased into arm (1) by adjusting the precision short. V_i is then the response of the initially unbalanced detector. Unbalancing the bridge only by changing the attenuator lets (II-25) become

$$V_i = K_0 (\delta\alpha)^2 \qquad \text{II-26}$$

Now let the phosphor sample be illuminated, so that there are additional small shifts in attenuation $\Delta\alpha$, and phase $\Delta\beta$. The resulting detector response V is from (II-24)

$$V = K_0 \left[(\delta\alpha + \Delta\alpha)^2 + \Delta\beta^2 \right] \qquad \text{II-27}$$

experimentally it is found that

$$(\delta\alpha + \Delta\alpha) \gg \Delta\beta$$

therefore

$$V^{1/2} - V_i^{1/2} = K_0^{1/2} \Delta\alpha$$

which when combined with (II-23) yields for the photocon-

ductivity

$$V_2^{1/2} - V_1^{1/2} = \frac{k_0^{1/2} \mu_0 \omega t}{a \beta_D} \Delta\sigma$$

$$= k_1 (\sigma - \sigma_0) \qquad \text{II-28}$$

where ($\sigma - \sigma_0$) is the photoconductivity and K_1 is an overall constant.

The above shows that the increase in conductivity due to light excitation is directly proportional to the difference in the square roots of the signals observed at the detector.

It is shown in Appendix C that the bridge is more sensitive when it is initially unbalanced.

III. Experimental Results

A. Sample

Most of the phosphor powders used in this experiment were prepared at the New York University Solid State Laboratory. Pure laboratory grade zinc or cadmium sulfide, together with the desired weight fractions of impurities were fired at 1150°C for two hours in a nitrogen atmosphere. Replacement of air by nitrogen prevented partial surface oxidation of the phosphor to CdO or ZnO, which are conducting. The phosphors used, the concentrations of activators and coactivators, and the wavelength at maximum luminescent emission are listed in Table I. A letter-number code designates the phosphors that were studied in this experiment. The code was originated at the New York University Solid State Laboratory to identify the phosphor powders at the time of their preparation.

The electric field strength in the phosphor ranged (from power measurements and Equation II-8) between 10 and 15 volts/cm. Changes in the magnitude of the electric field did not effect the measurements. All measurements were made at room temperature.

It is perhaps advisable to emphasize here that the photoconductivity was computed (Equations II-23 and II-28)

TABLE I

Phosphor Composition and Wavelength at Which Maximum Luminescence Occurs

Phosphor	Type	Wavelength for Max Luminescence Å	Activator %	Coactivator %
J-7	ZnS	5300	0.005 Cu	1 Cl
J-27*	ZnS	5300	0.005 Cu	1 Cl
R-130	ZnS	5200	0.1 Cu	1 Cl
R-134	ZnS	4700	Self Activated	
R-153	CdS	Not Measured	0.005 Cu	0.1 Cl
R-158	CdS	Not Measured	0.005 Cu	0.001 Cl
R-210	ZnS	5300	0.005 Cu	0.1 Al
R-305	ZnS	4700	0.005 Ag	1 Cl
LG-2150	ZnS	5300	0.003 Cu, 0.04 Pb	Cl+

*J-7 and J-27 have the same composition, but were prepared at different times.
+Percentage unknown.

from measured changes in the phase and attenuation of the microwave signal, and from the reading of the microwave bridge detector when the bridge was off balance. The order of magnitude of the measurements made with the microwave bridge at balance for all phosphors except LG2150, with uncertainties are h=(0.2 $\pm$ 10%) db; h=(0.01 $\pm$ 25%) db; x=(0.0030 $\pm$ 0.2%) meter; x ($3 \times 10^{-6} \pm$ 50%) meter. The uncertainty in the computation of the absolute photoconductivity is therefore from Equation II-23 about 35%. Experimental uncertainty with the unbalanced microwave bridge was 5%.

B. Dark Conductivity

All measurements of photoconductivity were made relative to a dark value which is the lowest value that could be obtained either by a long wait in the dark or by the use of quenching infrared radiation.

The dark value of the conductivity cannot be separated from the imaginary part of the permittivity. The quantity $\sigma_r + \omega\epsilon_0 K\rho_L$ (derived from Equation II-19) can be expressed in terms of the changes in attenuation and phase. To determine $\sigma_r + \omega\epsilon_0 K\rho_L$ (and thus an upper limit to the dark conductivity) the following experiment was carried out: The slotted waveguide section which served as the

sample holder was rotated through 90° with the addition of a waveguide twist section. Two glass plates, cemented together, were inserted into the sample holder with the microwave bridge at balance. The necessary attenuation, α_g, and phase change, β_g, required to rebalance the bridge were recorded. Dry desiccated phosphor powder was then sprinkled uniformly (in the dark) on the glass plates. This caused an additional attenuation change $\Delta\alpha_g$ and phase change $\Delta\beta_g$.

The quantity $\sigma_r + \omega\epsilon_0 k_{pi}$ was measured for two powders, an unactivated unfired ZnS and J-27. In both cases the quantity was approximately 2×10^{-3} (ohm-cm)$^{-1}$. This upper limit to σ_r, assuming that the mobility is[1] 10^{-2} m^2 (volt-sec)$^{-1}$, corresponds to a free electron density of 2.5×10^{12} electrons/cm^2. Since the same number is obtained for the activated and unactivated sample, the $\omega\epsilon_0 k_{pi}$ term may dominate, so that N is probably considerably less than 2.5×10^{12} electrons/cm^3. These dark measurements were very difficult to perform because the changes $\Delta\alpha_g$ and $\Delta\beta_g$ are close to the noise level.

C. Dependence of Photoconductivity on Excitation Intensity

The photoconductivity of ZnS and CdS phosphors is usually expressed by a power law[24] dependence on the

incident exciting irradiation:

$$\sigma - \sigma_o = k_\sigma I^n \qquad \text{III-1}$$

where σ_o is the dark conductivity, I is the intensity of exciting radiation, and k_σ is a constant. Equation (III-1) may be combined with Equation (II-28) to express this dependence in terms of experimental observables.

$$V^{1/2} - V_d = k_I I^n \qquad \text{III-1}$$

where K_I is a constant

Although application of Equation (III-2) on experimental observables will give a value for the exponent n , it cannot be used to determine absolute photoconductivity.

The null method described in Section II was used to determine the absolute photoconductivity when the phosphor was illuminated by light of maximum intensity. At lower intensities of excitation the photoconductivity was found from the experimentally determined value of n (using Equation III-2), the null determination referred to above, and Equation (III-1).

Figure III-1 shows the value of the conductivity change as a function of uv exciting intensity (3660Å) for six different ZnS phosphors, two of which were measured for different sample thickness. The slope, n , from the conductivity-excitation relationship (Equation III-1) ranged from n=0.23 to n=0.83. In general, the samples with the

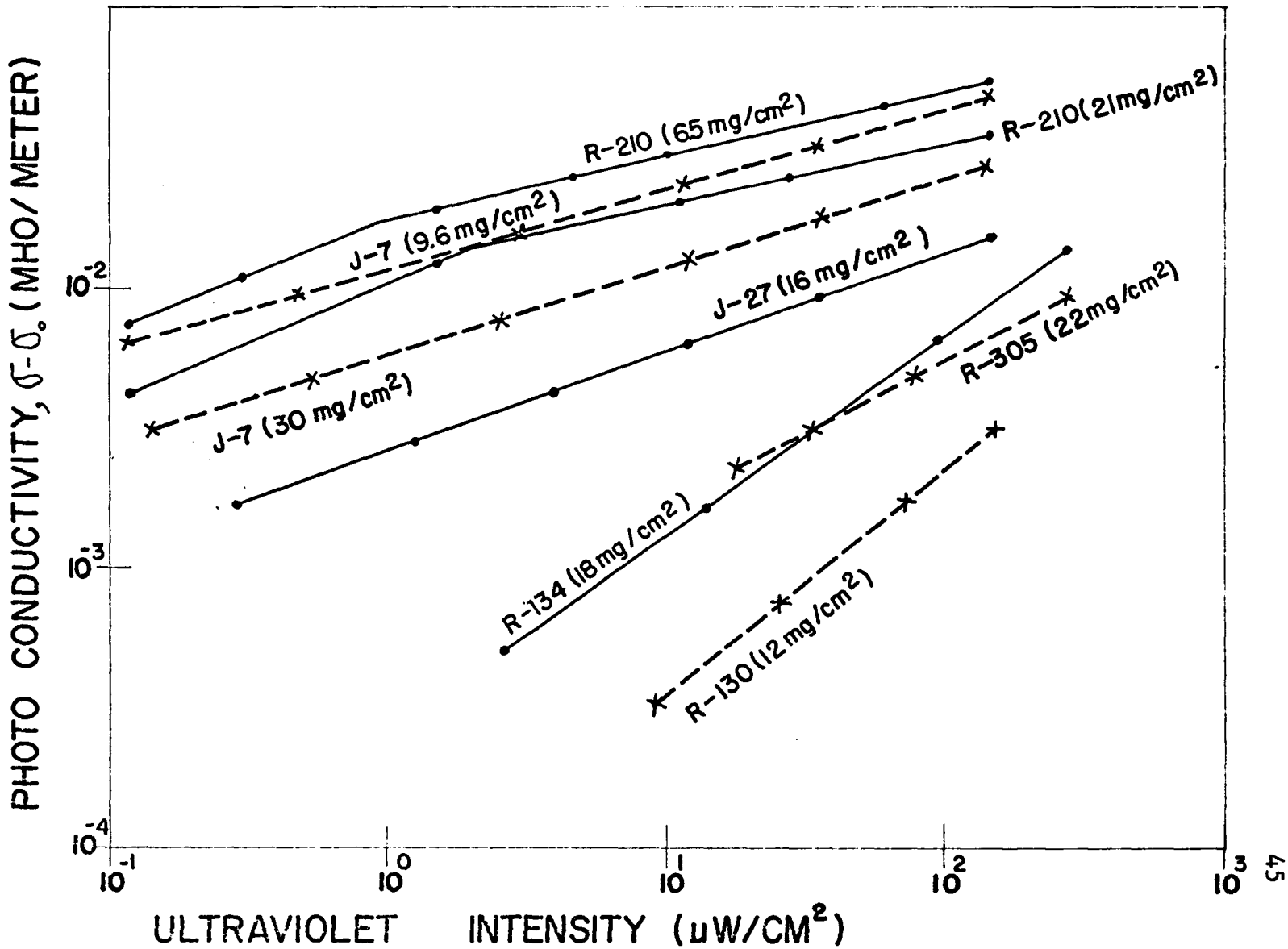

Figure III-1: Photoconductivity vs Ultraviolet Intensity for ZnS Phosphors. Ultraviolet excitation band centered at 3650Å.

smallest photoconductive response show the greatest slopes. For the R-210 phosphors there is an indication that the slope increases at the lowest applied intensities. However, measurements at these low intensity ranges are not very precise. The exponent in the conductivity-excitation relationship has previously been found to vary between 0.5 and 1 except for a superlinear relationship over a limited range of intensity[39]. The values of n less than 0.5 reported here for the ZnS: Cu and ZnS: (Al) activated phosphors are quite unusual.

The samples showing the greatest photoconductivity are the copper-activated material: R-210, J-7 and J-27. However, when a considerably greater amount of copper is added (R-130), the photoconductivity is reduced by about one order of magnitude. A self-activated and a silver-activated sample show intermediate photoconductive responses. For samples R-210 and J-7 the curves for the thicker samples are shifted to the right; that is, a higher intensity is required to obtain the same value of $\sigma - \sigma_o$. This is likely due to nonuniform excitation of the sample.

To further investigate this nonhomogeneous absorption, a R-210 phosphor sample was excited by light of various wavelengths (all on the long wavelength side of the absorption edge at 3400Å): λ = 3650Å, λ = 3900Å and λ = 4350Å.

It was found that the slope was independent of the excitation wavelength.

Similar conductivity measurements were made on CdS powders R-153 and R-158: The variation of conductivity change with excitation intensity is shown in Figure III-2. R-158 was excited at the absorption edge (λ = 5150Å). The slope varied between 0.79 at low levels and 0.52 at high levels of illumination. This discontinuous change in n has been observed[40] previously for CdS phosphors and can be explained with the Schon-Klasens model. It is surprising that R-153 (which differs from R-158 in coactivator concentration only) shows no discontinuity in slope.

In the case of R-153 three excitation wavelengths were used. The first was weakly absorbed (λ = 5500Å), the second was at the absorption edge (λ = 5150Å), and the third was strongly absorbed (λ = 4800Å) . As known, the response is strongest at the absorption edge, but it is remarkable that for all three types of excitation the slope is not very different ($0.68 < n < 0.84$) with the longest wavelength resulting in the highest slope.

Table II summarizes the photoconductivity of all the powders measured. Since the electron mobility of these materials is 100 cm^2/sec volt, the induced change in the density of the free electrons can be obtained and is given

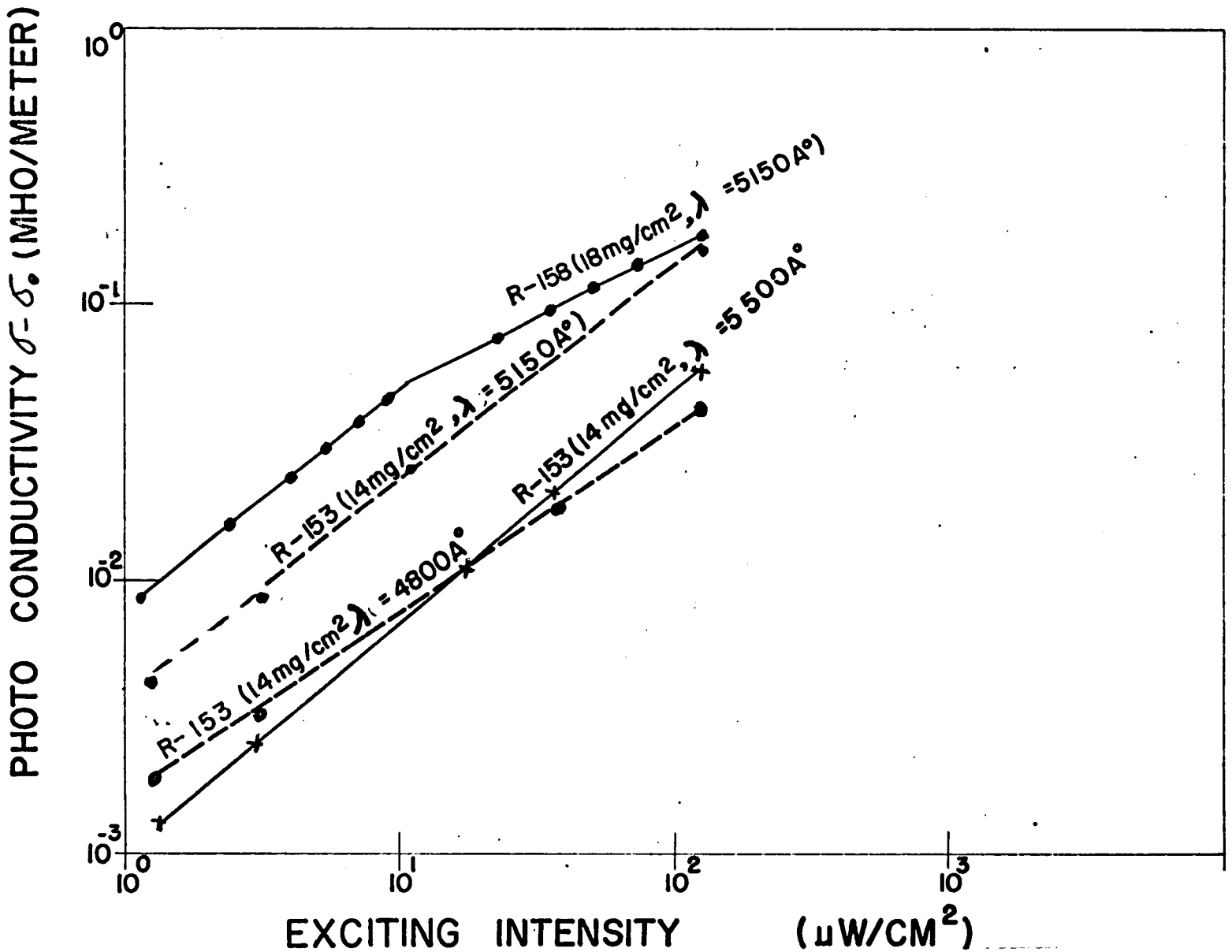

Figure III-2: Photoconductivity vs Intensity of Exciting Light for CdS Phosphors. Wavelength of excitation is shown on curve.

TABLE II

Photoconductivity of Various ZnS and CdS Samples

Phosphor	Powder Density mg/cm^2	Excitation Wavelength	Incident Intensity $\mu w/cm^2$	Change in Electron Density[a] $(10^{12}/cm^3)$	Slope (n)
J-7	9.8	3660Å	140	30	0.29
J-7	30	3660Å	140	17	0.32
J-27	16	3660Å	150	10	0.36
R-130	12	3660Å	150	2	0.83
R-134	18	3660Å	280	9	0.72
R-210	6.5	3660Å	140	36	0.23 0.40*
R-210	21	3660Å	140	23	0.24 0.43*
R-305	22	3660Å	275	6	0.52
LG-2150	20	3660Å	280	0.5	Not Measurable
R-153	14	4800Å	125	26	0.68
R-153	14	5150Å	125	100	0.78
R-153	14	5500Å	125	35	0.84
R-158	18	5150Å	125	115	0.52 0.79*

(a) The change in the electron density was obtained from the conductivity by assuming that the mobility = $100 cm^2/Volt\text{-}sec$.

* Slopes in the lowest intensity range.

in Column 5.

To compare the CdS results with those of the ZnS materials only the long wavelength excitation of the former should be considered. The photoconductive response of R-153 (CdS) and J-7 and R-210 (ZnS) are then seen to be approximately equal.

LG-2150 (ZnS;Cu,Pb,Cl) does not show any measurable photoconductivity at microwave frequencies. A.C. measurements done at low frequency on this phosphor (100 - 10,000 Hz) show a measurable response,[27] indicating that at these low frequencies the trapped electrons have sufficient time to evaporate and follow the field but that the actual equilibrium number of free electrons is very small in the field-free situation.

Theoretical calculations leading to values of $n < 0.5$ have previously been reported. Rose[12] finds that if the insulator or semiconductor has been highly sensitized by the addition of more than one class of discrete states, the conductivity-intensity curve is likely to have a slope n 0.5. Klasens[39] obtains the condition n = 1/3 only when the light emission $\mathcal{L} \propto I_{uv}^{2/3}$; certainly this is not the case with these measurements. Moss[41] derives a 1/3 power law assuming highly absorbed excitation; it is doubtful that this condition is fulfilled when ZnS is excited by $\lambda = 3660\text{Å}$.

Kallmann and Kramer[12] show that a dependence n = 1/3 is obtained when the number of traps is comparable to or less than the number of conduction electrons. Since the former is at least of the order of $10^{16}/cm^3$ (as determined by rise curve and glow curve measurements) this condition does not hold in the experiments reported here.

The exponent in the luminescence-exciting uv intensity relation and the wavelength at which the luminescence was sampled are given in Table III. It is seen that the luminescence varies almost linearly with ultraviolet intensity for each of these materials.

D. Dependence of Photoconductivity on Wavelength

The spectral dependence of photoconductivity was investigated for two CdS powders. A high intensity Bausch and Lomb Grating Monochrometer was used in conjunction with a high pressure Xenon lamp as the light source. The unbalanced bridge method was used to measure photoconductivity. Readings were taken in steps of 0.05 microns, the half-width of the instrument being 0.01 microns. Glass plates were interposed between the monochrometer and the phosphor to attenuate the light, as needed, to effect a constant intensity over the entire spectral range of exciting irradiation.

Results for R-153 and R-158 are given in Figures III-3

TABLE III

Exponent in Power Law Dependence of Luminescence on Ultraviolet Intensity For ZnS Phosphors ($\mathcal{L} = k_{\lambda} I_{uv}^{n_1}$)

Phosphors	n_1	Wavelength of Luminescence Sampled
J-7	1.03	5100Å
J-27	0.98	5100Å
R-130	0.97	5100Å
R-134	1.20	5100Å
R-210	0.97	5100Å
R-305	0.91/1.21	5100Å/4300Å

and III-4. The spectral response shows a sharp peak at 5150Å, i.e., near the absorption edge, with a much lower flat maximum at long wavelengths, where the intrinsic absorption drops, and a fairly rapid fall at short wavelengths.

E. Simultaneous Ultraviolet and Infrared Radiation

As mentioned earlier, it is known[42] that in the steady state additional infrared reduces the uv induced light emission and conductivity in many (Zn;Cd)S materials. This decrease in conductivity, commonly referred to as quenching, Q_σ, is defined as $Q_\sigma = \frac{(\sigma-\sigma_o)_{uv} - (\sigma-\sigma_o)_{uv+ir}}{(\sigma-\sigma_o)_{uv}}$ where $(\sigma-\sigma_o)_{uv}$ is the equilibrium conductivity under ultraviolet irradiation and $(\sigma-\sigma_o)_{uv+ir}$ is the equilibrium conductivity under concommitant ultraviolet and infrared irradiation. The percent quenching, % Q_σ, is defined by

$$\% Q_\sigma = \frac{(\sigma-\sigma_o)_{uv} - (\sigma-\sigma_o)_{uv+ir}}{(\sigma-\sigma_o)_{uv}} 100$$

Quenching of luminescence, Q_L, and percent quenching of luminescence, % Q_L, are similarly defined. According to The Schon-Klasens model, this quenching is due to the release of positive holes trapped at activator sites and their subsequent recombination (partly nonradiative) with trapped or conduction electrons. A direct comparison of the infrared quenching on luminescence and photoconductivity

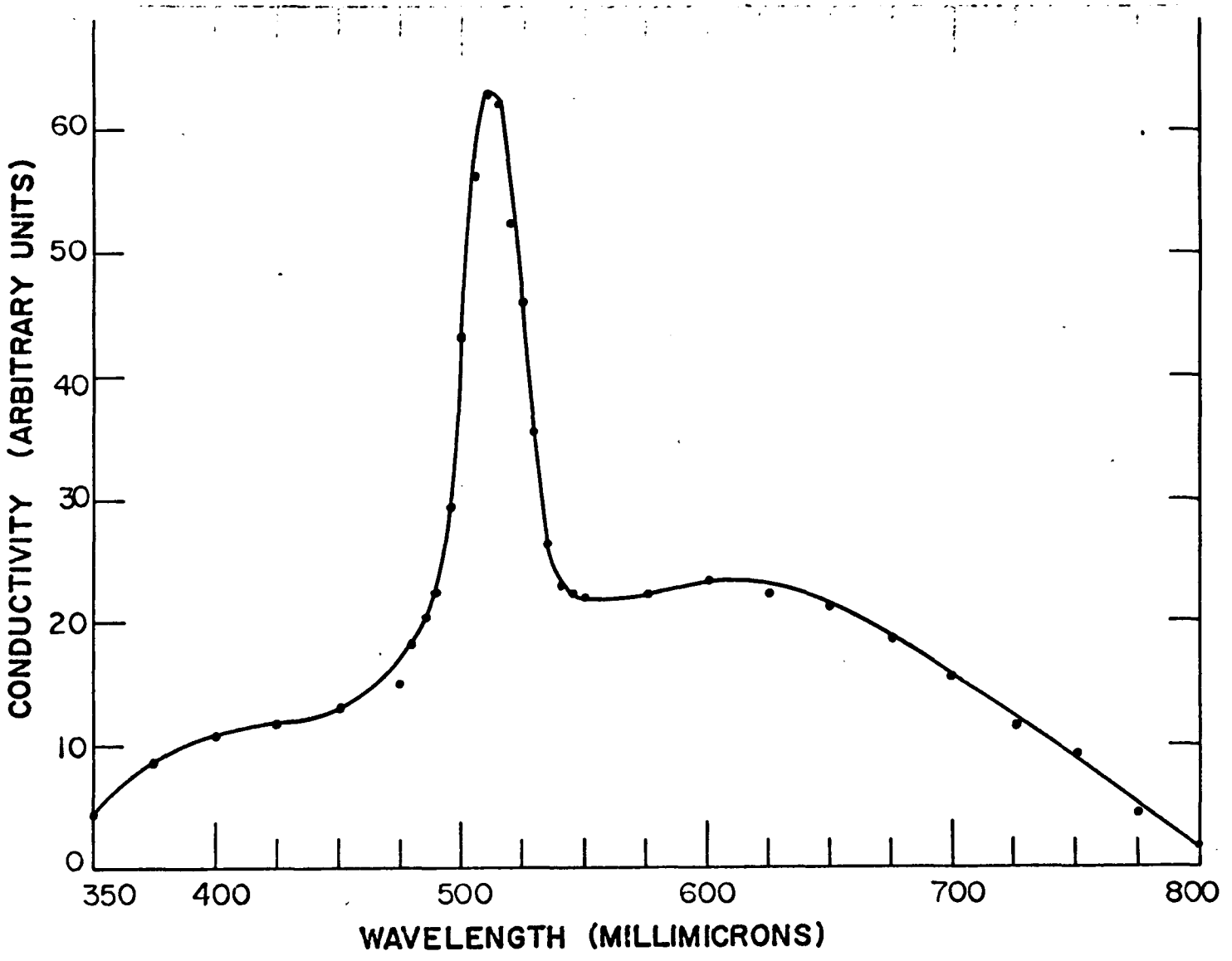

Figure III-3: Spectral Response of Photoconductivity for R-153 CdS Phosphor. Intensity was 125 $\mu W/cm^2$ throughout spectral range. Peak of curve corresponds to conductivity of 0.16 mho/meter.

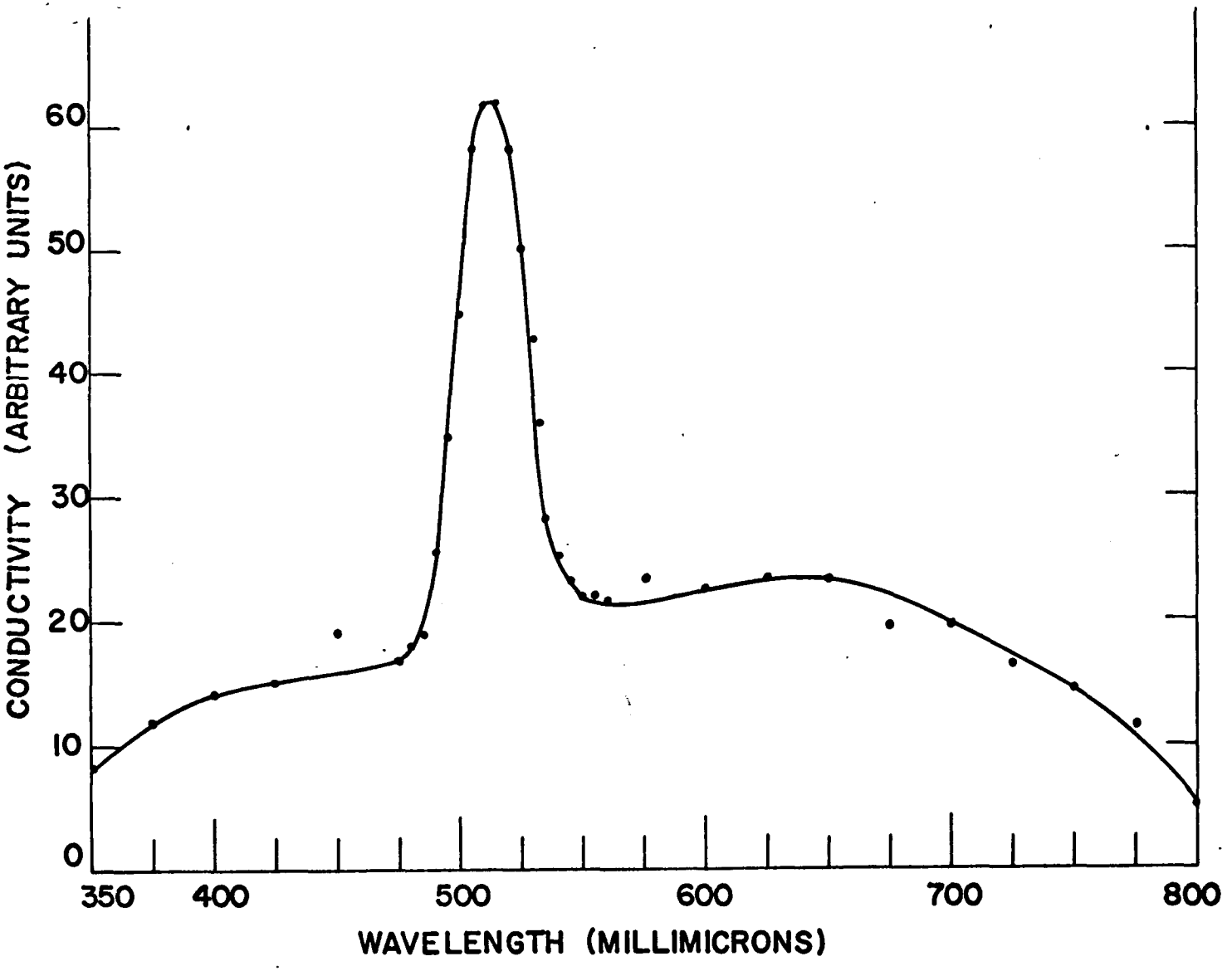

Figure III-4: Spectral Response of Photoconductivity for R-158 CdS Phosphor. Intensity was 125 $\mu W/cm^2$ throughout spectral range. Peak of curve corresponds to conductivity of 0.18 mho/meter.

could lead to some conclusions on the transitions involved, but previous methods of conductivity are subject to the errors discussed in Section I. At microwave frequencies, these difficulties are eliminated.

It was found in the experiments reported here that infrared radiation alone (in the range of 7000Å - 8000Å) induces a measurable, lasting photoconductivity for J-7, J-27 and R-210. Although this induced conductivity is relatively small compared to that induced by uv excitation of the same incident intensity, a correction is required in the usual quenching expression. It is assumed that this correction is independent of the uv excitation. The values of quenched conductivity in Tables III through VII include a correction to account for this ir excitation.

Table IV gives the quenching of both luminescence and photoconductivity observed when infrared (two 7-69 Corning Filters: λ_{ir} = 8000Å, 6.6 mw/cm^2) is added to various levels of uv excitation for five phosphors. With ZnS activated with copper the quenching of the photoconductivity is greater than the luminescent quenching; for the self-activated (R-134) phosphor no conductivity quenching is observed although some luminescence quenching is noted at low exciting intensities.

For the silver-activated phosphor the quenching of

TABLE IV

Quenching of Luminescence (Q_L) and Photoconductivity (Q_σ) by Infrared (8000Å, 6.6mw/cm^2) at Various Ultraviolet (3660Å) Intensities

Iuv $\mu w/cm^2$	ZnS:Cu, Cl J-27		ZnS:Cu, Al R-210		ZnS:Cu, Cl R-130		ZnS R-134		ZnS:Ag, Cl R-305	
	$\%Q_L$	$\%Q_\sigma$	$\%Q_L$	$\%Q_\sigma$	$\%Q_L$	$\%Q_\sigma$	$\%Q_L$	$\%Q_\sigma$	$\%Q_L$	$\%Q_\sigma$
155	7.9	27	16	30	1.8	2.0	0	0	11	11
45	18	37	25	37	3.2	7.3	0	0	19	22
10	22	48	40	49	5.9	24	40	-	35	-
4.0	31	59	47	*	12	30	8.0	-	46	-
1.0	42	60	61	64	16	-	9.0	-	59	-
0.3	64	75	76	71	39	-	-	-	-	-

* NO MEASUREMENT MADE
\- NOT MEASURABLE

luminescence and of conductivity are comparable at higher exciting intensities. Conductivity measurements could not be obtained for lower uv exciting intensities. It is seen that the luminescent quenching for this phosphor is in the same range as that of the copper activated samples. Moreover, the self-activated and silver-activated samples differ from the copper-activated samples in that the latter show considerably more conductivity quenching. This indicates that a mechanism valid for one type of activator may not hold for another, a result also indicated by polarization studies of luminescence[43].

It was noted that of all these phosphors except R-134 (self-activated), the quenching of the luminescence as a function for the uv excitation can be approximated by $\% Q_L = 100/ (1 + cI_{uv}^{\frac{1}{2}})$. J-27 and R-210, containing the same amount of copper activation, but different coactivators are remarkably similar as regards luminescence and conductivity quenching. R-130, which has a larger copper concentration, has a smaller quenching effect in both luminescence and conductivity, contrary to the results of Meyer[44] in which increased luminescent quenching occurred with higher copper content.

To examine the light and conductivity quenching at different wavelengths, a monochromator was used (resulting

in a lower ir intensity). Tables Va and Vb give the results of the quenching for two ZnS Cu-activated phosphors, J-7 and R-210, at wavelengths of 7500Å, 10,000Å and 12,000Å over a range of uv intensities. For both phosphors, the quenching of both luminescence and conductivity is larger for 7500Å and 12,000Å and smaller for 10,000Å as has been previously reported[45]. The conductivity quenching is greater than that of the luminescence for all wavelengths, and the quenching increases with decreasing uv excitation. No conductivity quenching was observed for R-134 (self-activated) or R-305 (Ag, Cl) at any of these three wavelengths.

To determine the effect of the sample thickness on luminescence and conductivity quenching, measurements were made with a 30 mg/cm^2 and a 9.8 mg/cm^2 sample of J-7 under various levels of uv excitation using 7500Å and 8500Å ir irradiation. Table VIa shows that the percent quenching of these two samples is, under identical conditions, approximately the same. However, the ratio $\%\,Q_r / \%\,Q$ shows a marked difference when comparisons are made between the two samples. The ratio is almost invariably greater for the thicker sample. This is not unexpected since the measured conductivity is primarily a bulk effect while the measured luminescence is primarily a surface effect. Conductivity quenching is known to increase under weaker uv

TABLE Va

J-7 (9.8 mg/cm^2)

Quenching at Various Infrared Wavelengths, ir Intensity 0.47 mw/cm^2

Iuv	7500Å		10,000Å		12,000Å	
μw/cm^2	$\%Q_L$	$\%Q_\sigma$	$\%Q_L$	$\%Q_\sigma$	$\%Q_L$	$\%Q_\sigma$
67	0.2	17	0	3.6	0	6.5
45	0.5	19	*	*	1.2	6.0
12	4.5	30	0.4	10	1.2	9.8
1.7	11	41	3.2	12	3.2	17
0.45	22	42	6.3	15	8.8	23

TABLE Vb

R-210 (21 mg/cm^2)

Quenching at Various Infrared Wavelengths, ir Intensity 0.3 mw/cm^2

Iuv	7500Å		10,000Å		12,000Å	
μw/cm^2	$\%Q_L$	$\%Q_\sigma$	$\%Q_L$	$\%Q_\sigma$	$\%Q_L$	$\%Q_\sigma$
145	3.4	17	1.7	3.9	1.7	4.4
40	5.0	22	1.8	7.7	2.2	9.8
10	9.7	31	3.4	14	6.2	16
4.3	14	37	3.7	17	7.2	25
1.8	22	41	6.0	22	9.0	25
.34	29	54	17	20	20	33

* No Measurement Made

TABLE VIa

Light and Conductivity Quenching of J-7 (30 mg/cm^2 and 9.8 mg/cm^2), ir Intensity 0.45 mw/cm^2

J-7: 30 mg/cm^2 and 9.8 mg/cm^2 (in brackets)

Iuv(7-83) w/cm^2	% Q_L		% Q_σ		% Q_σ/% Q_L	
	λ_{ir} = 7500Å	λ_{ir} = 8500Å	λ_{ir} = 7500Å	λ_{ir} = 8500Å	λ_{ir} = 7500Å	λ_{ir} = 8500Å
140	- (2.0)	- (1.0)	9.0 (9.0)	7.9 (7.5)	- (4.5)	- (7.5)
39	1.5 (3.0)	1.5 (1.5)	16 (14)	16 (12)	10.7 (4.7)	10.7 (8.0)
9.0	2.7 (5.0)	2.7 (4.7)	27 (22)	23 (18)	10 (4.4)	8.5 (3.8)
3.4	5.3 (9.0)	5.3 (6.0)	30 (26)	24 (21)	5.7 (2.9)	4.5 (3.5)
1.3	13 (14)	10 (11)	30 (30)	27 (22)	2.3 (2.1)	2.7 (2.0)
0.30	30 (27)	20 (21)	34 (37)	32 (28)	1.1 (1.4)	1.6 (1.3)

- NOT MEASURABLE

excitation (which is expected in the sample interior) and therefore the ratio referred to above would increase with sample thickness. Nevertheless, a 3 to 1 difference in sample thickness does not induce appreciable errors in the quenching measurements. High intensity (6.6 mw/cm^2) ir radiation at 8000Å on two different thicknesses of R-210 (6.5 mg/cm^2 and 21 mg/cm^2) resulted in similar quenching for each phosphor sample. The data are shown in Table VIb.

Table VII gives the quenching for phosphor J-7 as a function of the ir intensity (λ ir = 8000Å with the excitation level remaining constant (I = 2.5 μW/cm^2). The quenching increases with increasing ir intensity but not at a linear rate. Thus, when the intensity increases from 30 μW/cm^2 to 260 μW/cm^2, $\%Q_L$ increases by a factor of 2.5 and %Q by a factor of 2.0. With a further tenfold increase of ir intensity (to 2700 W/cm^2), $\%Q_L$ increases by a factor of 3.4 and $\%Q_\sigma$ by a factor of about 2.0. Previous measurements[46] had indicated a leveling-off process in which the quenching reaches a value less than 100%.

The conductivity quenching is again greater than the luminescent quenching at all ir values but the ratio $\%Q_\sigma/Q_L$ decreases with increasing ir intensity. This indicates that a very high ir intensities % Q_σ and % Q_L would be the same.

TABLE VIb

Light and Conductivity Quenching of R-210 (21 mg/cm^2 and 6.5 mg/cm^2), ir Intensity 6.5 mW/cm^2 at λ_{ir}=8000Å
R-210 21 mg/cm^2 and 6.5 mg/cm^2 (in brackets)

Iuv(7-83) w/cm^2	$\%Q_L$	$\%Q_\sigma$	$\%Q_L$ / $\%Q_\sigma$
145	14 (16)	29 (30)	2.07 (1.87)
40	20 (25)	41 (37)	2.05 (1.48)
10	32 (40)	52 (49)	1.63 (1.23)
36	43 (47)	55 -	1.28 (-)
.9	53 (61)	- (64)	- (1.05)

TABLE VII

Conductivity and Luminescence Quenching of J-7 ($30mg/cm^2$) as a Function of ir Intensity (two 7-69 Filters Plus 25cm of Water), $I_{uv} = 2.5\ \mu w/cm^2$

ir Intensity $\mu w/cm^2$	$\%Q_L$	$\%Q_\sigma$	$\%Q_\sigma / \%Q_L$
30	4.0	11	2.7
115	7.1	14	2.0
260	10	21	2.1
520	16	25	1.6
1400	27	34	1.3
2700	34	40	1.2
4500	40	55	1.4

F. Rise and Decay of Photoconductivity and Luminescence

The time dependent behavior of the photoconductivity and luminescence was observed using the equipment described in Section II. A recorder was used to display the information.

Figures III-5 and III-6 show the rise and decay curves of J-7 (14 mg/cm^2) for excitation by 4400Å (7 μW/cm^2) and 3600Å (0.11 μW/cm^2) respectively. After approximately 15 minutes of decay, ir was applied and a faster decrease was noted in the conductivity.

The conductivity rise and decay times are considerably larger than those of luminescence. In the case of stronger excitation (Figure III-5) it is seen that thirty minutes after the excitation is removed the luminescence is less than 1% of the equilibrium value while the conductivity is about 30% of the equilibrium value. This is not due to any drift in the microwave apparatus since the addition of infrared brings the conductivity back to the zero level.

In the case of the weakly excited phosphor the conductivity is still 70% of its equilibrium value forty minutes after excitation is removed while the luminescence has decreased to less than 0.1% of its equilibrium value in the same time. Addition of infrared brings the conductivity to 20% of its equilibrium level. This indicated re-

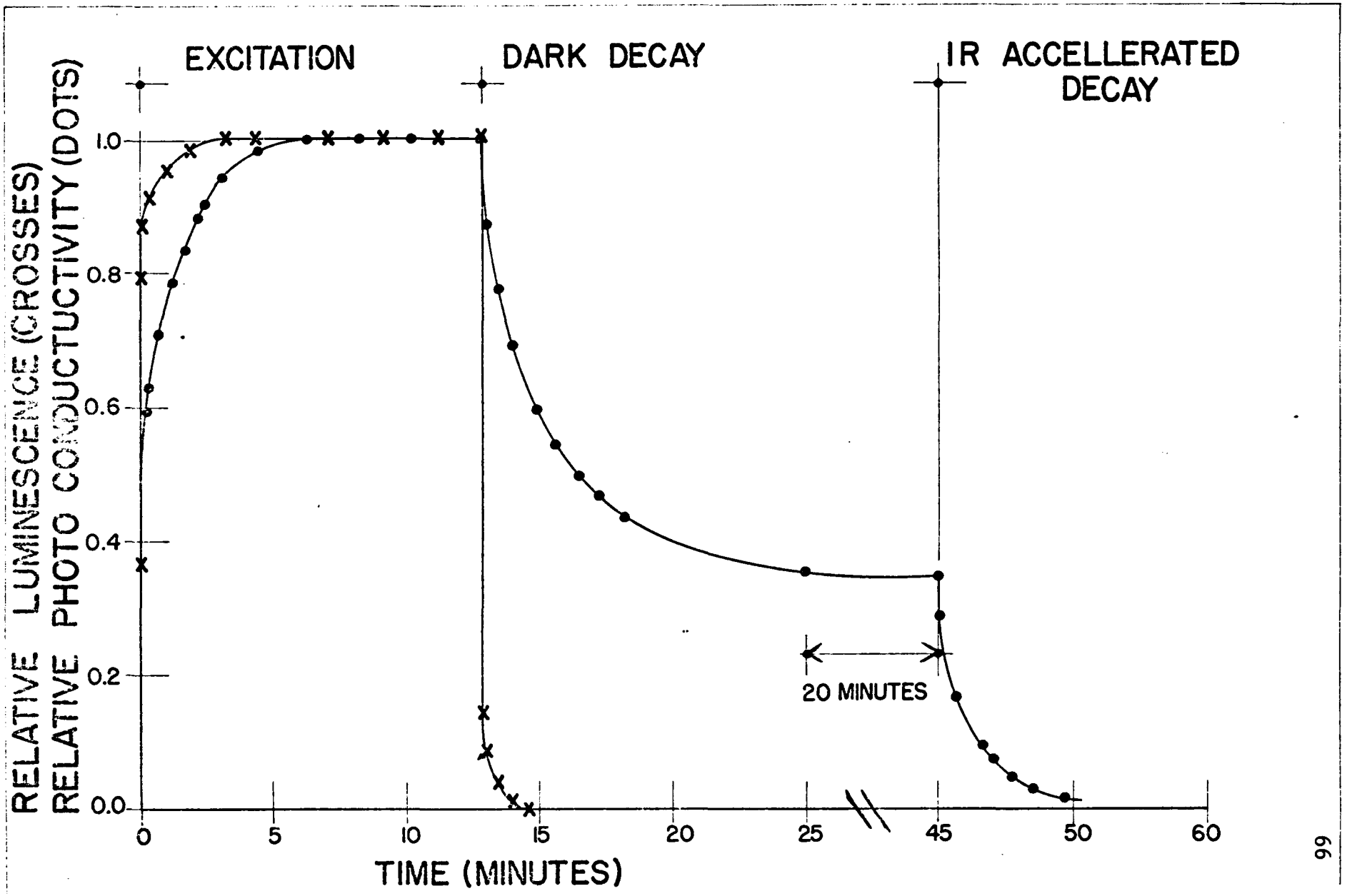

Figure III-5: Rise and Decay of Photoconductivity and Luminescence for J-7 (14 mg/cm^2) Phosphor. Excitation by 4400Å light at 7.3 μW/cm^2. Long wavelength ir ($\lambda_{ir} \geq$ 9000Å) at 600 μW/cm^2 was used to accelerate the decay.

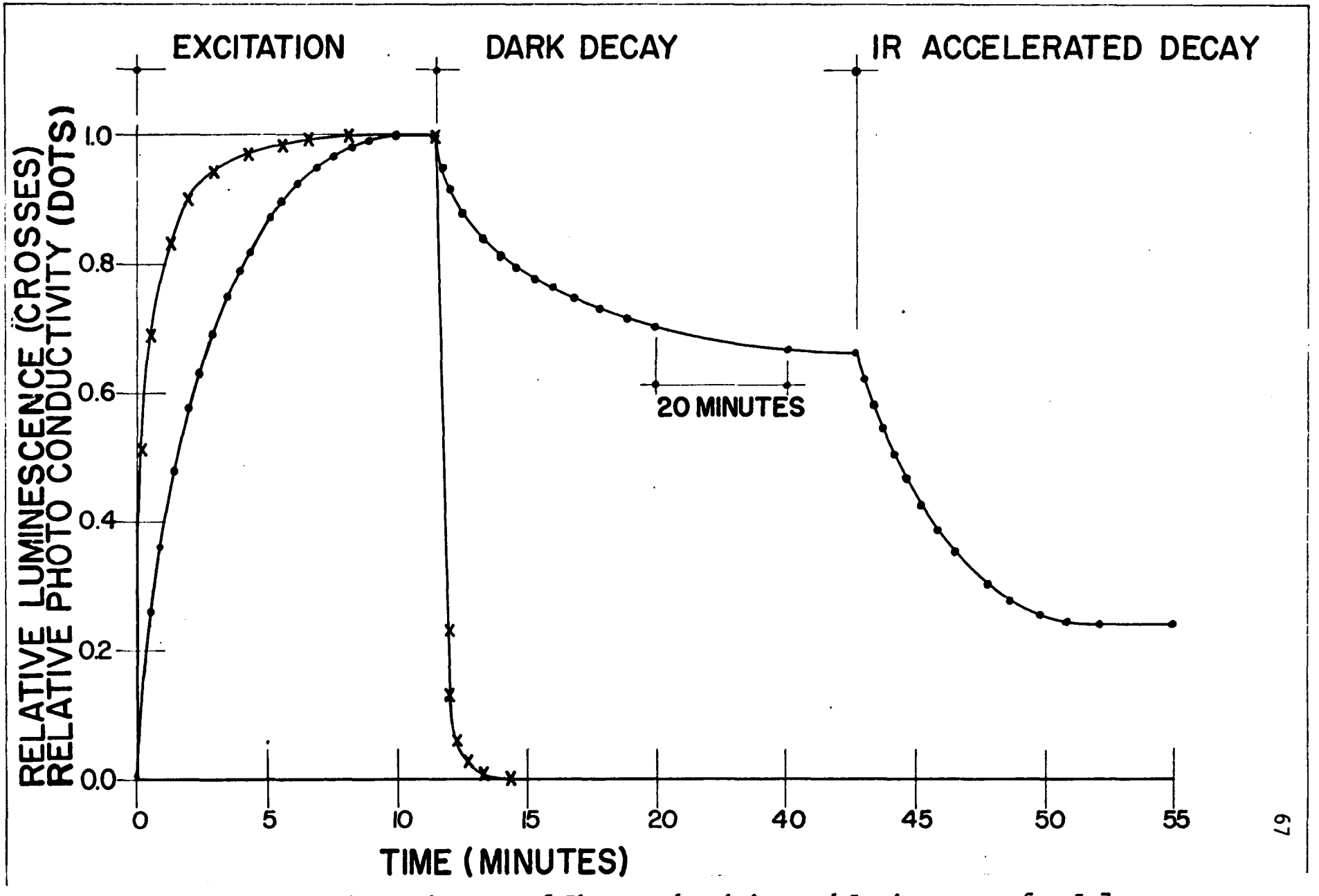

Figure III-6: Rise and Decay of Photoconductivity and Luminescence for J-7 (14 mg/cm^2) Phosphor. Excitation by 3650Å light at 0.11 μW/cm^2. Long wave- [illegible] at 600 μW/cm^2 was used to accelerate decay.

sidual (fractional) conductivity is quite small in absolute terms since the phosphor was irradiated with the lowest uv intensity radiation used in these experiments.

Time dependent quenching measurements are shown in Figures III-7 and III-8. All quenching radiation was 8000Å at high intensity. In each case the photoconductivity and luminescence were allowed to reach their equilibrium values before the ir was added. The values of uv exciting intensity were 1.35 and 29 uw/cm^2 respectively. As expected, quenching was greatest for the least excited phosphor. It is also seen that the quenching process takes more time to reach equilibrium (and recover) for lower uv exciting intensity. The luminescent process is again faster than the photoconductive process.

When the ir is initially switched on a fast rise (stimulation) of conductivity and luminescence is seen for low uv intensity (Figure III-7). The effect is more marked for the least excited phosphor in the experiment described here. A drop only in conductivity is observed when the ir is switched off. However[7], others have observed a decrease in both conductivity and luminescence. These phenomena are not observed at higher uv exciting intensities (see Figure III-8) because they are relatively small compared to the equilibrium values.

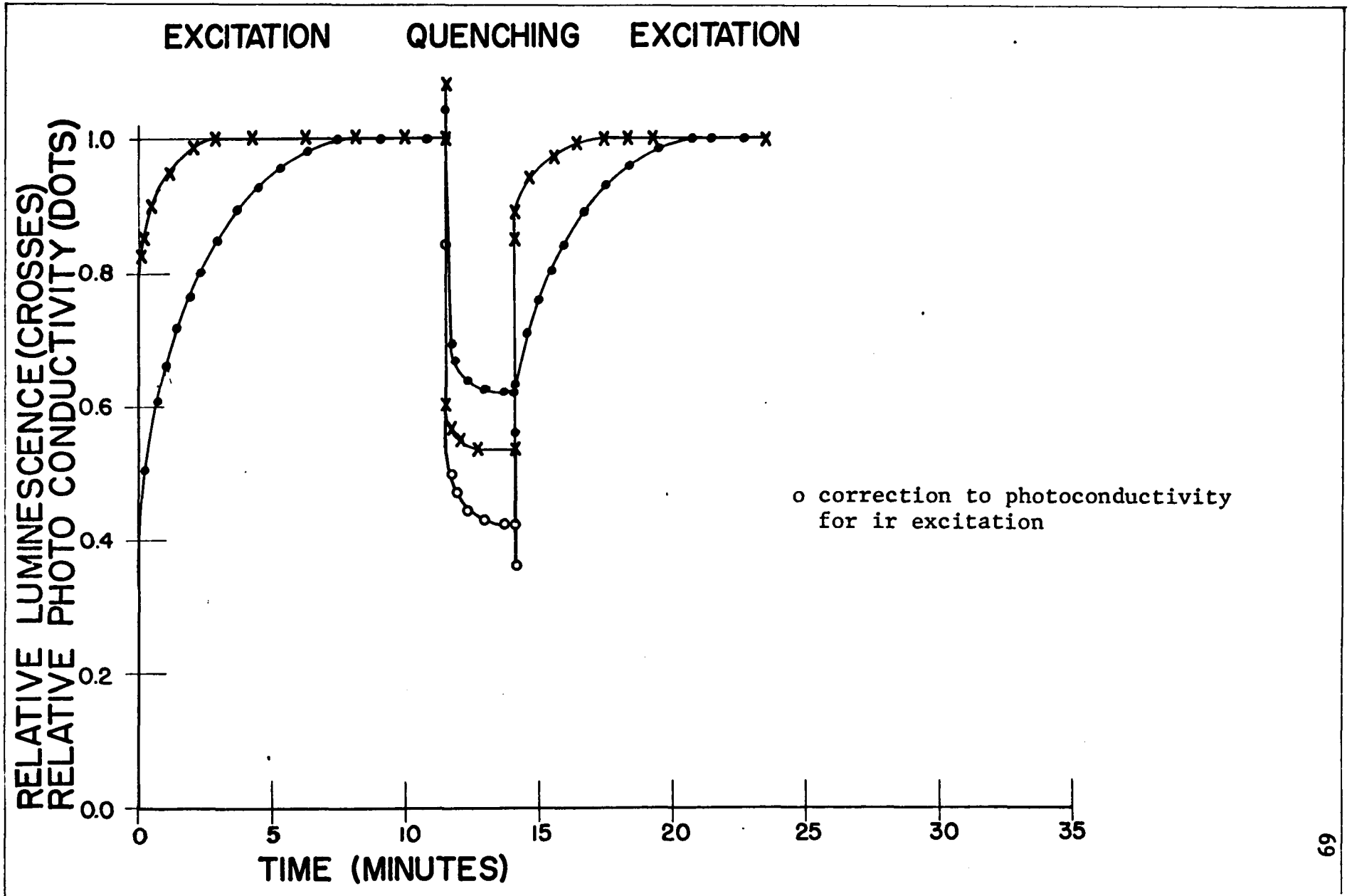

Figure III-7: Quenching of Photoconductivity and Luminescence by Infrared as a Function of Time for J-7 (14 mg/cm^2) Phosphor. Excitation by 3650Å at 1.35 W/cm^2. [illegible] quenching wavelengths and intensity 8000Å and 6600 W/cm^2 respectively.

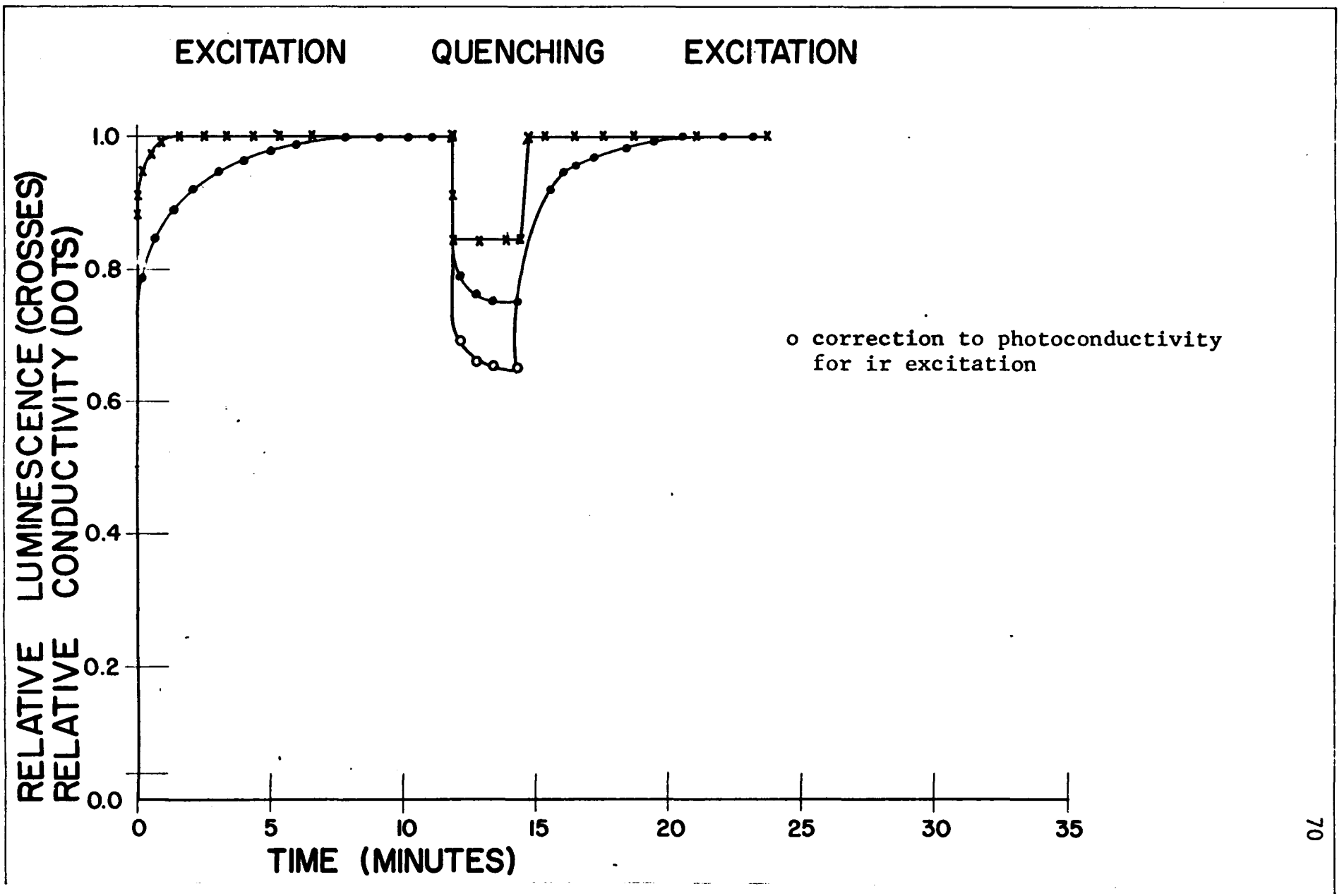

Figure III-8: Quenching of Photoconductivity and Luminescence by Infrared as a Function of Time for J-7 (30 mg/cm^2) Phosphor. Excitation by 3650Å at 29 μW/cm^2. Infrared quenching wavelength and intensity 8000Å and 4475 W/cm^2 respectively.

Figure III-9 shows rise and decay curves of R-130, the more heavily doped Cu-activated phosphor. The quenching effects of 8000Å radiation at 6.6 mw/cm^2 is also shown. The transients due to ir are seen to be faster, but less extensive than those observed with J-7 under similar experimental conditions (see Figure III-8).

Table VIII summarizes the rise and decay times observed with the various samples. It is clear that the rise time of the conductivity is longer than that of the luminescence for all the phosphors measured except R-130 where the rise time for both was below 0.1 min.

The most extensive series of measurements was made with J-7 and the table shows that:

a. Decreasing the excitation intensity increases both rise times (T_L and T_σ);

b. Increasing the thickness increases both rise times;

c. Increasing the excitation wavelength increases both rise times.

These results are not unexpected, since (a), (b), and (c) all effectively result in a decreased absorbed energy, so that a longer period of excitation time is required to bring the sample to its equilibrium value.

For J-7, T_L is much more dependent on the intensity

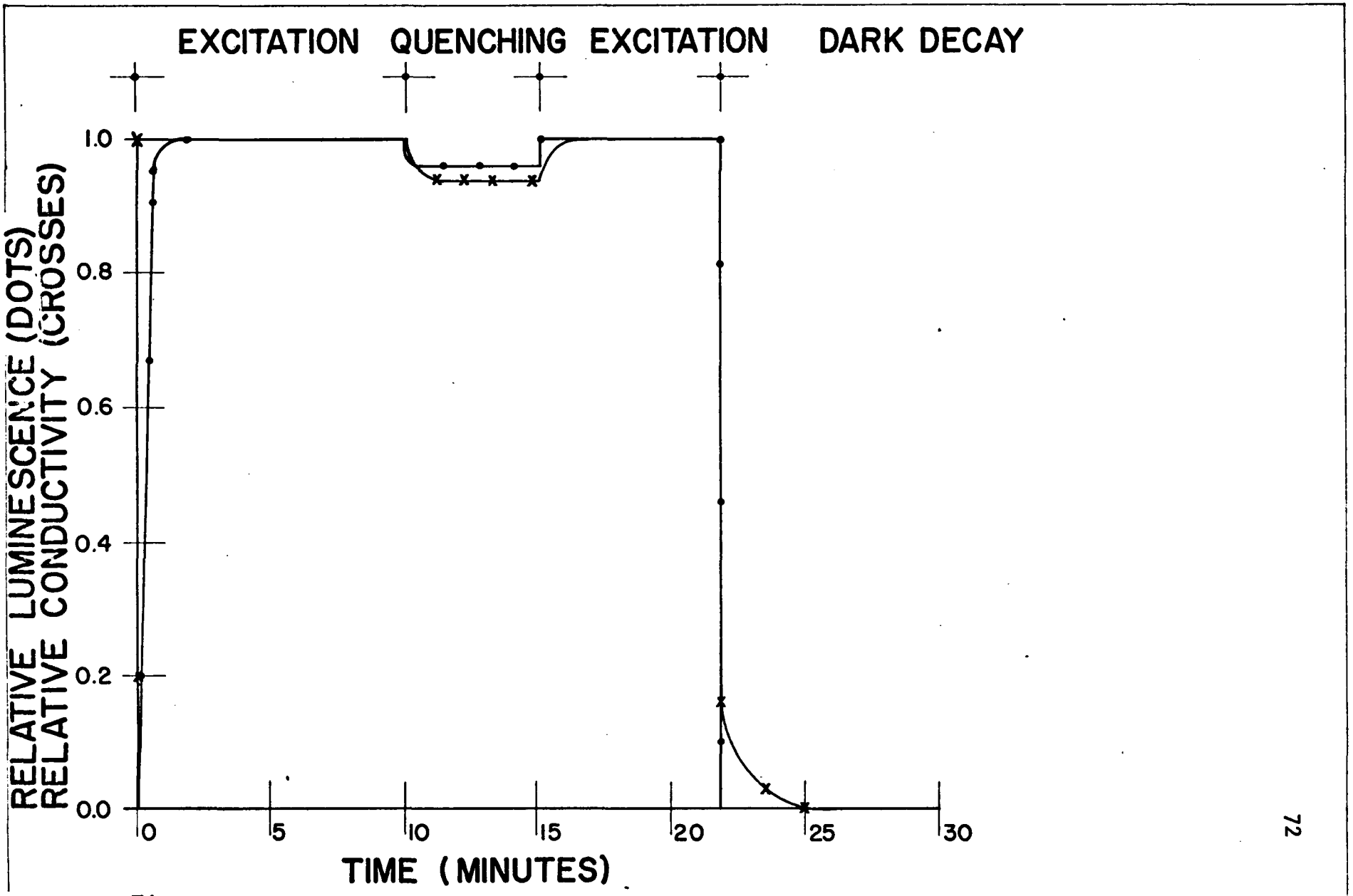

Figure III-9: Rise, Quenching and Decay of Photoconductivity and Luminescence as a Function of Time for R-130 (12.3 mg/cm^2) Phosphor. Excitation by 3650Å at 29 W/cm^2. Infrared quenching wavelength and intensity 8000Å and 6600 W/cm^2 respectively

TABLE VIII

Rise time of Photoconductivity (τ_σ) and Luminescence (τ_L) to reach 0.9 of the equilibrium value, and decay time to decrease to 0.5 of the equilibrium value for various phosphors

PHOSPHOR	DENSITY mg/cm^2	FILTER+	Iuv μw/cm^2	RISE (MIN) τ_L	RISE (MIN) τ_σ	DECAY (MIN) τ_L	DECAY (MIN) τ_σ
J-7	14	7-83	1.35	0.6	4.0	*	*
J-7	14	7-83	0.11	2.0	5.5	~0.1	>40
J-7	30	7-83	29	0.5	2.0	<0.1	0.5
J-7	30	7-83	0.93	1.0	7.7	*	*
J-7	30	7-83	0.20	4.5	11.5	*	*
J-7	14	5-74	7.3	0.2	27	~0.1	16
J-7	14	5-74	0.58	4.5	10.5	*	*
R-134	6.1	7-83	3.6	0.1	0.5	<0.1	~0.3
R-305	21	7-83	42	0.1	0.1	<0.1	~0.2
R-305	21	7-83	3.6	0.1	0.5	<0.1	~0.5
R-130	12	7-83	42	0.1	0.1	<0.1	~0.1

* NO MEASUREMENT MADE

\+ 7-83 passes 3660Å
5-74 passes 4300Å

than T_{σ} . Thus, for the 14 mg/cm^2 sample a decrease in uv excitation by a factor greater than 10 increases T_L by a factor of 3, but T increases only by 40%. A similar effect is seen for the thicker sample (lines 4 and 5) and for excitation with blue light (lines 6 and 7). This is not unexpected since the conductivity depends only weakly on the intensity as shown in the equilibrium measurements (See Figures III-3 and III-4).

IV. Discussion of Results and Conclusions

The experiments described here have shown that a microwave bridge can be used to detect a change in the propagation characteristics of electromagnetic waves passing through ZnS and CdS phosphors as a consequence of excitation. The inherent advantages of this technique (elimination of contact and barrier potentials, minimal disturbance of trap populations and elimination of grain polarization) over others provides a better means for the measurement of photoconductivity.

The photoconductive response of the CdS phosphors R-153 and R-158 as a function of exciting intensity and wavelength as measured in these experiments is similar to prior measurements [7,11,16,18] made on CdS crystals and phosphors.

The most extensive measurements were made on ZnS phosphors. Photoconductivity and luminescence measurements made concomittantly have resulted in a number of important observations:

1. For the commonly investigated ZnS:Cu,Cl, and ZnS:Cu,Al green emitting phosphors, the photoconductivity shows only a weak dependence on the excitation over a wide range of incident intensities while the luminescence is linearly dependent. In the equation $(\sigma-\sigma_0) \propto I^n$, n is

experimentally found to vary between 0.23 and 0.36 (Table II). This is considerably below values to be expected from the Schon-Klasens model which leades to values depending on whether traps are saturated or not.

2. For all the phosphors measured, the equilibrium quenching of the photoconductivity is greater or equal to the quenching of the luminescence. The Schon-Klasens model, where:

$$L = \beta n_c p_t \qquad \text{IV-1}$$

(L the luminescence, β the transition probability, n_c the density of free electrons, and P_t the density of trapped holes) predicts that the luminescence will be reduced more than the photoconductivity because both n_c and P_t are reduced by the infrared.

3. For all samples measured, a comparison of the rise and decay times of the luminescence and the photoconductivity shows that the former always has a shorter time constant as seen in Table VIII. Using the Schon-Klasens model, one can write

$$\frac{L}{L_o} = \frac{n_c p_t}{n_{co} p_{to}}$$

where the zero subscript indicates the equilibrium value. During both the rise and decay $L/L_o < n_c/n_{co}$ since P_t/P_{to} is always less than 1. The expected luminescence rise and decay curve always falls below that of the photoconductivity

curve (where both are normalized to their equilibrium values) and thus has a longer rise time and a faster decay time. Experimentally it is found that the time constant associated with the luminescence is faster than that associated with photoconductivity for both the rise and decay period.

It is clear that these experimental observations cannot be explained by the Schon-Klasens model. However, forward way, and to account for these discrepancies. This can be done by using the Prenner-Williams assumption that luminescent centers have a range of radiative recombination probabilities.[47] This is similar to the assumption that the luminescent transitions occur from shallow traps to the ionized activators. The luminescence still has the dependence shown in Equation IV-1 if the number of shallow traps is taken to be equal to the number of trapped holes.[7] β , the recombination probability is no longer a constant but depends on intensity, addition of infrared, and time after excitation or interruption of excitation.

If depends on the excitation intensity, it should be larger for greater excitation intensities, since strong

excitation results in saturation of the slowly recombining centers, causing a larger fraction of the fast recombination centers to be operative. Thus, in Equation IV-1 one can replace β by $\bar{\beta}$ where $\bar{\beta}$ is some average recombination constant which increases with exciting intensity. In the range where traps are far from saturated the Schon-Klasens model predicts

$$n_c^2 = k I_{uv} / \bar{\beta}$$

This causes the exponent n in the relationship $\sigma - \sigma_0 \propto I_{uv}^{n}$ to be less than one-half; the exact value determined by the dependence of $\bar{\beta}$ on Iuv.

Examining the ratio of quenched to unquenched luminescence at equilibrium, the following is obtained:

$$L_{uv+ir} / L_{uv} = \left(\bar{\beta}_{uv+ir} / \bar{\beta}_{uv} \right) \left(n_{c\,uv+ir} / n_{c\,uv} \right) \left(P_{t\,uv+ir} / P_{t\,uv} \right)$$

For constant $\bar{\beta}$,

$$L_{uv+ir} / L_{uv} \leq n_{c\,uv+ir} / n_{c\,uv}$$

since the ratio

$$P_{t\,uv+ir} / P_{t\,uv}$$

is always less than or equal to one. However, if $\bar{\beta}_{uv+ir}$ becomes considerably larger than $\bar{\beta}_{uv}$ the luminescence quenching may become considerably less than the current

quenching, as observed in these experiments.

Transfer of electrons from traps to the conduction band (and to a lesser degree holes from activator sites to the valence band) explains the stimulation of conductivity. In the steady state, however, the transfer of holes to faster recombination (radiation and radiationless) sites results in conductivity quenching. This reordering of the activator hole population to faster centers is equivalent to a larger $\bar{\beta}$.

When infrared radiation is applied, holes are excited from activator sites to the valence band. These free holes may be captured by a fast center. This, in effect, transfer holes from slow centers to fast ones, giving rise to momentary increase in luminescence. The equilibrium quenching of luminescence occurs because the holes excited to the valence band are also be captured by non-radiative centers and because the free electron density is reduced.

Finally, the rise and decay times will be discussed. As soon as excitation is applied the fast recombination centers pay the dominant role, but as equilibrium is reached $\bar{\beta}$ decreases since both types (fast and slow centers) are now involved. Thus, the luminescence curve may rise more quickly than that of the conductivity because of the larger initial values of $\bar{\beta}$ as observed in Table VII. In

the decay, as observed above, the luminescence should decrease more rapidly than the conductivity even if $\bar{\beta}$ remains constant. If $\bar{\beta}$ decreases (since only the long-time centers remain active), the luminescence will decay even more rapidly than expected from the unmodified Schon-Klasens model. In fact, Shionoya and co-workers[49] assuming a bi-molecular recombination kinetics, interpreted their data as indicating that $\bar{\beta}$ decreases with time, and reaches a constant during the latter part of the decay curve.

For the experiments described in this paper, the modification of the Schon-Klasens model based on changes of $\bar{\beta}$ seems to be adequate. The separate activator and sensitizing levels proposed recently[3] are not required for the results reported here.

Appendix A

Calculation of Conductivity by a Perturbation Method

This appendix shows how the conductivity of the phosphor sample may be related to the propagation constant of the electromagnetic field in the sample. The criteria for neglecting higher order evanescent modes[50] $\left(\epsilon(\epsilon-1)\frac{a}{\lambda\pi}\frac{\omega^2}{c^2} \ll \pi\right)$ is easily satisfied in this calculation.

The waveguide section containing the phosphor as seen in Figure (A-1) may be considered to consist of five layers. Two air layers of complex relative permittivity ϵ_a and thickness $\frac{a}{2} - t_g + \frac{t}{2}$, two glass layers of complex relative permittivity ϵ_g and thickness t_g, and a phosphor layer of dark (nonilluminated) complex permittivity ϵ_p. The thickness of the phosphor layer is t. The overall length of the obstacle is L. Its height, b, and depth, a, are respectively equal to the length of the long and shortwave guide walls. The tapering angle with the axis is θ.

The expressions for the electromagnetic field in the nonilluminated section of the waveguide containing the phosphor sample are from (II-1)

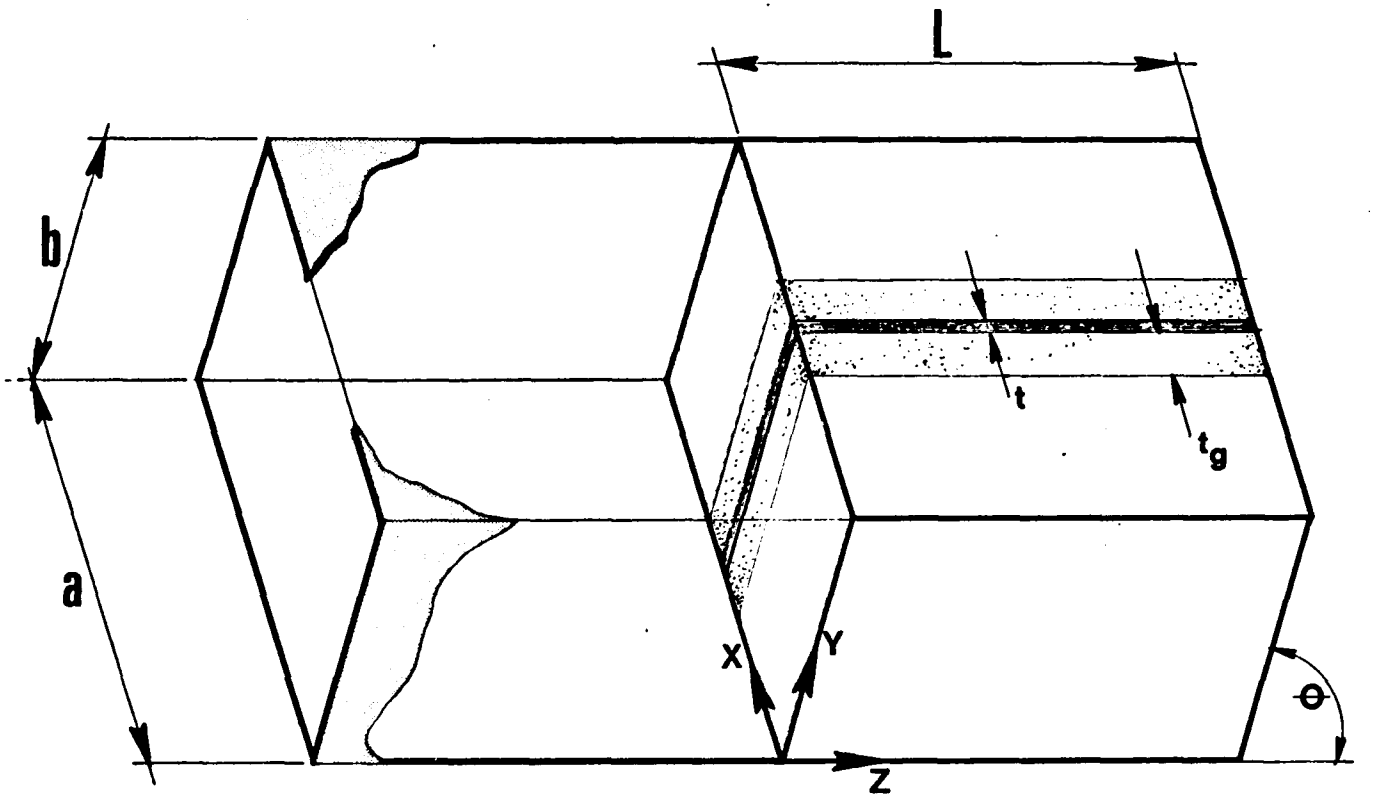

Figure A-1: Perspective View of Wave Guide Obstacle.

$$E_x = E_z = H_y = 0$$

$$\vec{E}_y = E_o \sin\frac{\pi x}{a}\, e^{-\gamma_D z + j\omega t}\, \vec{j}$$

$$H_x = \frac{j\gamma_D}{\omega\mu_o} E_o \sin\frac{\pi x}{a}\, e^{-\gamma_D z + j\omega t}\, \vec{i} \qquad \text{A-1}$$

$$H_z = \frac{j\pi}{a\,\omega\mu_o} E_o \cos\frac{\pi x}{a}\, e^{-\gamma_D z + j\omega t}\, \vec{k}$$

Here E_o is the amplitude of the electric field for $z = o$, as measured from the origin in Figure A-1. $\vec{i}$, $\vec{j}$, and $\vec{k}$ are the conventional rectangular coordinate unit vectors, and γ_D, as before, is the effective propagation constant.

The vector identity

$$\vec{\nabla}\cdot(\vec{E}\times\vec{H}^*) = \vec{H}^*\cdot\vec{\nabla}\times\vec{E} - \vec{E}\cdot\vec{\nabla}\times\vec{H}^*$$

in conjuction with Maxwell's Equations

$$\nabla\times\vec{E} = -\mu_o\frac{\partial\vec{H}}{\partial t} \quad ; \quad \nabla\times\vec{H} = \vec{J} + \epsilon_o\epsilon\frac{\partial\vec{E}}{\partial t}$$

and Gauss's theorem combine to give the expression

$$\oint_S (E_y H_z^*\,\vec{i} - E_y H_x^*\,\vec{k})\cdot d\vec{S}$$

$$= -\int_V \left(\mu_o\vec{H}^*\cdot\frac{\partial\vec{H}}{\partial t} + \vec{E}\cdot\vec{J}^* + \epsilon\epsilon_o\vec{E}\cdot\frac{\partial\vec{E}^*}{\partial t}\right) dv \qquad \text{A-2}$$

Here the volume integration V is over the interior of the waveguide and the surface integration S is over the surface bounding the volume V.

Making use of Eq. (II-18) and (A-1), the right hand side of equation (A-2) becomes

$$\text{RHS (A-2)} = \int\left(-j\omega\mu_o\vec{H}^*\cdot\vec{H} - \sigma^*\vec{E}\cdot\vec{E}^* + j\omega\epsilon\epsilon_o\vec{E}\cdot\vec{E}^*\right) dv$$

which upon substitution for the fields from (A-1) becomes

$$\text{RHS (A-2)} = \iint \frac{j\omega\mu_0\gamma_D\gamma_D^*}{\mu_0^2\omega^2} E_0^2 \sin^2\left(\frac{\pi x}{a}\right) e^{-(\gamma_D+\gamma_D^*)z} - j\omega\mu_0\left(\frac{\pi}{a}\right)^2\frac{E_0^2}{\omega^2\mu_0^2}\cos^2\left(\frac{\pi x}{a}\right)e^{-(\gamma_D+\gamma_D^*)z} + E_0^2\sin^2\left(\frac{\pi x}{a}\right)e^{-(\gamma_D+\gamma_D^*)z}\Big] \left[j\omega\epsilon\epsilon_0 - \sigma^*\right]\Big\} dv$$

$$= \frac{j}{\mu_0\omega}\int\Big[\Big\{\mu_0\omega^2\epsilon\epsilon_0 + j\mu_0\omega\sigma^* - \gamma_D\gamma_D^*\Big\}E_0^2\sin^2\left(\frac{\pi x}{a}\right)e^{-(\gamma_D+\gamma_D^*)z} - \left(\frac{\pi}{a}\right)^2 E_0^2\cos^2\left(\frac{\pi x}{a}\right)e^{-(\gamma_D+\gamma_D^*)z}\Big]dv \qquad \text{A-3}$$

Now $dv = dx\,dy\,dz$ and the limits of integration are (from Figure 3-2)

$y = 0$ to $y = b$

$x = 0$ to $x = a$

$z = y/\tan\theta$ to $z = L + y/\tan\theta$

Substituting the above into Eq. (A-II) and integrating with respect to z there results

$$\text{RHS (A-3)} = \int\Big[\Big\{\mu_0\omega^2\epsilon\epsilon_0 + j\mu_0\omega\sigma^* - \gamma_D\gamma_D^*\Big\}\sin^2\frac{\pi x}{a} - \left(\frac{\pi}{a}\right)^2\cos^2\frac{\pi x}{a}\Big]\Big\{e^{-(\gamma_D+\gamma_D^*)(L+y/\tan\theta)} - e^{-(\gamma_D+\gamma_D^*)y/\tan\theta}\Big\}dx\,dy \qquad \text{A-4}$$

Consider now the surface integral on the left hand side of Equation (A-2). The term involving the unit vector $\vec{i}$ is over the yz surfaces of the waveguide where $\vec{E} = 0$. These surfaces lie at $x = 0$ and $x = a$, and since $E_y = 0$ for $x = 0$, $x = a$, there is no contribution to the surface integral from the first term on the left hand side of (A-2). The left hand side of (A-2) therefore reduces to

$$\text{LHS (A-2)} = -\oint E_y H_x^* \vec{k}\cdot\vec{ds} \qquad \text{A-5}$$

The unit vector $\vec{\kappa}$ is parallel to the nontapered faces of the obstruction and therefore only the surface integrals over the tapered faces contribute to (A-5). Now $\vec{\kappa}\cdot d\vec{s}$ $= -dx\,dy$ for the near tapered face and $\vec{\kappa}\cdot d\vec{s} = dx\,dy$ for the far tapered face. As before $z = +\frac{y}{\tan\theta}$ for the near tapered face and $z = L + \frac{y}{\tan\theta}$ for the far tapered face. Equation (A-5) with substitutions from (A-1) becomes

$$-\oint E \times H^{*}\cdot\vec{\kappa}\cdot d\vec{s} = \frac{jE_o^2}{\omega\mu_o}\gamma^{*}\int_{\text{tapered faces}} \sin^2\frac{\pi x}{a}\, e^{-(\gamma_D+\gamma_D^{*})z}\,dx\,dy$$

$$= \frac{jE_o^2\gamma^{*}}{\omega\mu_o}\int\left[\sin^2\frac{\pi x}{a}\left\{e^{-(\gamma_D+\gamma_D^{*})\left(\frac{y}{\tan\theta}+L\right)} - e^{-(\gamma_D+\gamma_D^{*})\frac{y}{\tan\theta}}\right\}dx\,dy \qquad \text{A-6}$$

where as before x varies from o to a and y varies from o to b.

Inspection of Equations (A-4) and (A-6) shows that the terms of the integrands involving y are identical. Therefore the integrals over y factor out. Equating (A-4) and (A-6) one has

$$-\frac{jE_o^2}{\mu_o\omega(\gamma_D+\gamma_D^{*})}\int_{x=o}^{a}\left[\left\{\mu_o\omega^2\epsilon\epsilon_o + j\mu_o\omega\sigma^{*} - \gamma_D\gamma_D^{*}\right\}\sin^2\frac{\pi x}{a} - \left(\frac{\pi}{a}\right)^2\cos^2\frac{\pi x}{a}\right]dx$$

$$= \frac{jE_o^2}{\mu_o\omega}\gamma^{*}\int_{x=o}^{a}\sin^2\frac{\pi x}{a}\,dx \qquad \text{A-7}$$

Integrating all terms not having coefficients of ϵ and σ, yields

$$\left[\gamma_D^* (\gamma_D + \gamma_D^*) - \left(\frac{\pi}{a}\right)^2 - \gamma \gamma^* \right] \frac{a}{2}$$

$$= - \mu_0 \omega^2 \epsilon_0 \int_{x=0}^{a} \epsilon \operatorname{sen}^2 \frac{\pi x}{a} \, dx - j \mu_0 \omega \int_{x=0}^{a} \sigma^* \operatorname{sen}^2 \frac{\pi x}{a} \, dx \qquad A-8$$

The first integral on right hand side of Equation (A-8) may now be broken up into three integrals, one for each value of ϵ. The second integral has no contribution from the glass and air volumes since the conductivity of glass and that of air is taken to be zero. Equation (A-8) then becomes

$$\left[\gamma_D^* \gamma_D^* - \left(\frac{\pi}{a}\right)^2 \right] \frac{a}{2}$$

$$= - 2 \mu_0 \omega^2 \epsilon_0 \left[\epsilon_a \int_{x=0}^{x=\frac{a}{2} - t_g - t/2} \operatorname{sen}^2 \frac{\pi x}{a} \, dx + \epsilon_g \int_{x=\frac{a}{2} - t_g - t/2}^{x=\frac{a}{2} - \frac{t}{2}} \operatorname{sen}^2 \frac{\pi x}{a} \, dx + \epsilon_p \int_{x=\frac{a}{2} - \frac{t}{2}}^{x=\frac{a}{2}} \operatorname{sen}^2 \frac{\pi x}{a} \, dx \right]$$

$$- 2 j \mu_0 \omega \int_{x=\frac{a}{2} - \frac{t}{2}}^{x=\frac{a}{2}} \sigma^* \operatorname{sen}^2 \frac{\pi x}{a} \, dx . \qquad A-9$$

Making use of the identity

$$\int \operatorname{sen}^2 \theta \, d\theta = \frac{1}{2} \theta - \frac{1}{4} \operatorname{sen} 2\theta$$

(A-9) becomes

$$\left[\gamma_D^* \gamma_D^* - \left(\frac{\pi}{a}\right)^2 \right] \frac{a}{2}$$

$$= - 2 \mu_0 \omega^2 \epsilon_0 \frac{a}{2\pi} \left[\epsilon_a \left\{ \frac{\pi}{a} \left(\frac{a}{2} - \left(t_g + \frac{t}{2} \right) \right) - \frac{1}{2} \operatorname{sen} \frac{\pi}{a} (a - 2t_g - t) \right\} \right.$$

$$+ \epsilon_g \left\{ \frac{\pi}{a} t_g + \frac{1}{2} \operatorname{sen} \frac{\pi}{a} (a - 2t_g - t) - \frac{1}{2} \operatorname{sen} \frac{\pi}{a} (a - t) \right\}$$

$$\left. + \epsilon_p \left\{ \frac{\pi}{a} \left(\frac{t}{2} \right) + \frac{1}{2} \operatorname{sen} \frac{\pi}{a} (a - t) - \frac{1}{2} \operatorname{sen} \frac{\pi}{a} a \right\} \right]$$

$$- j \mu_0 \omega \sigma^* \frac{a}{\pi} \left[\frac{\pi}{a} \frac{t}{2} + \frac{1}{2} \operatorname{sen} \frac{\pi}{a} (a - t) - \frac{1}{2} \operatorname{sen} \frac{\pi}{a} a \right]$$

$$= \mu_0 \omega^2 \epsilon_0 \left[\epsilon_a \frac{a}{2} + (\epsilon_g - \epsilon_a) \left\{ t_g + \frac{a}{2\pi} \operatorname{sen} \frac{\pi}{a} (a - 2t_g - t) \right\} \right.$$

$$\left. + (\epsilon_p - \epsilon_a) \frac{t}{2} + (\epsilon_p - \epsilon_g) \frac{a}{2\pi} \operatorname{sen} \frac{\pi}{a} (a-t) \right] \qquad \text{A-10}$$

$$- j \mu_0 \omega \sigma^* \left[\frac{t}{2} + \frac{a}{2\pi} \operatorname{sen} \frac{\pi}{a} (a-t) \right]$$

Using

$$\operatorname{sen} (A-B) = \operatorname{sen} A \cos B - \cos A \operatorname{sen} B$$

the preceding becomes

$$\left[\epsilon_0^* \gamma_0^* - \left(\frac{\pi}{a} \right)^2 \right] \frac{a}{2}$$

$$= -\mu_0 \omega^2 \epsilon_0 \left[\epsilon_a \frac{a}{2} + (\epsilon_g - \epsilon_a) \left\{ t_g + \frac{a}{2\pi} \operatorname{sen} \frac{\pi}{a} (2t_g + t) \right\} \right.$$

$$\left. + (\epsilon_p - \epsilon_a) \frac{t}{2} + (\epsilon_p - \epsilon_g) \frac{a}{2\pi} \operatorname{sen} \frac{\pi}{a} t \right]$$

$$- j \mu_0 \omega \sigma^* \left[\frac{t}{2} + \frac{a}{2\pi} \operatorname{sen} \frac{\pi}{a} t \right]$$

Now, since $a \gg t_g$, t, the sine functions may be expanded, resulting in

$$\left[\gamma_D^* \gamma_D^* - \left(\frac{\pi}{a}\right)^2\right] \frac{a}{2}$$

$$= -\mu_0 \omega^2 \epsilon_0 \left[\epsilon_a \frac{a}{2} + (\epsilon_g - \epsilon_a)\left\{2t_g + \frac{t}{2}\right\}\right.$$

$$\left. + (\epsilon_p - \epsilon_a)\frac{t}{2} + (\epsilon_p - \epsilon_g)\frac{t}{2}\right] - j\mu_0 \omega \sigma^* t .$$

Since

$$\gamma_D^* \gamma_D^* = \alpha_D^2 - \beta_D^2 - 2j\alpha_D \beta_D$$

, (A-10) becomes

$$\left[\alpha_D^2 - \beta_D^2 - 2j\alpha_D \beta_D - \left(\frac{\pi}{a}\right)^2\right] \frac{a}{2}$$

$$= -\mu_0 \omega^2 \epsilon_0 \left[\left(\frac{a}{2} - 2t_g - t\right)\epsilon_a + 2t_g \epsilon_g + \epsilon_p t\right] - \mu_0 \omega (j\sigma_r - \sigma_i) t$$

$$= -\mu_0 \omega^2 \epsilon_0 \left[\left(\frac{a}{2} - 2t_g - t\right)\epsilon_a + 2t_g (\epsilon_{gr} + j\epsilon_{gi}) + (\epsilon_{pr} + j\epsilon_{pi}) t\right] \qquad \text{A-11}$$

$$- \mu_0 \omega (j\sigma_r - \sigma_i) t$$

where σ, ϵ_g, and ϵ_p have been expressed in terms of real and imaginary parts. Equating real and imaginary parts of Equation (A-11) yields

$$a\alpha_D \beta_D = \mu_0 \omega \sigma_r t + \mu_0 \omega^2 \epsilon_0 (2t_g \epsilon_{gi} + t\epsilon_{pi}) \qquad \text{A-12}$$

$$\frac{a}{2}\left[\alpha_D^2 - \beta_D^2 - \left(\frac{\pi}{a}\right)^2\right] = -\mu_0 \omega^2 \epsilon_0 \left[\left(\frac{a}{2} - 2t_g - t\right)\epsilon_a + 2t_g \epsilon_{gr} + t\epsilon_{pr}\right] \qquad \text{A-13}$$

$$+ \mu_0 \omega \sigma_i t$$

The phase constant in the empty guide, β, is given by[51]

$$\mu_0 \omega^2 \epsilon_0 - \left(\frac{\pi}{a}\right)^2 = \left(\frac{2\pi}{\lambda_{g_0}}\right)^2 = \beta_0^2$$

Substituting the above in (A-13) and letting $\epsilon_a = 1$ results in

$$\frac{a}{2}\left[\beta_D^2 - \alpha_D^2 - \beta_o^2\right]$$

$$= \mu_o \omega^2 \epsilon_o \left[(\epsilon_{gr} - 1) 2t_g + (\epsilon_{pr} - 1)t - \frac{\tau}{\epsilon_o}\sigma_r t\right] \qquad \text{A-14}$$

$$\sigma_t = \omega \tau \sigma_r$$

where use has been made of

The perturbation calculation thus yields two equations, (A-12), (A-14), which relate the propagation characteristics of the microwave signal to the conductivity and permittivity of the sample. It is here emphasized that the conductivity as expressed in Equation (A-13) and (A-14) is for the dark, nonilluminated phosphor.

Appendix B

Nonuniform Excitation of Phosphor Sample

Equations II-21 and II-22 are exprssions derived for the photoconductivity under the implicit assumption that the density of exciting radiation remains constant throughout the interior of the phosphor. Here an expression is found for the photoconductivity where it is assumed that the intensity of exciting radiation has an exponential dependence on penetration depth.

The power dependence of photoconductivity on ultraviolet intensity is from III-2

$$\sigma - \sigma_0 = K_\sigma I_{uv}^{n} \qquad \text{B-1}$$

where σ_0 is the dark conductivity of the phosphor. The expression for the intensity of exciting radiation as a function of penetration x is

$$I(x) = I_0 e^{-\delta x} \qquad \text{B-2}$$

where I_0 is the intensity at the surface of the phosphor and δ is the attenuation constant. Combining B-1 and B-2 yields

$$\sigma(x) - \sigma_0 = K_\sigma I^{n}(x) = K_\sigma \left[I_0 e^{-\delta x} \right]$$

$$= K_\sigma I_0^{n} e^{-n\delta x}$$

or

$$\sigma(x) - \sigma_0 = \sigma(0)\, e^{-\eta \delta x} \qquad \text{B-3}$$

where $\sigma(o)$ is the photoconductivity at the surface of the illuminated phosphor.

Reference is now made to Equation A-9 which relates waveguide propagation constants to integral terms involving electromagnetic parametric constants of materials within the guide. Particular interest is attached to the third term, T_3 on the right hand side of Equation A-9 which is written here.

$$T_3 = -2j\mu_0\omega \int_{x=\frac{a}{2}-\frac{t}{2}}^{\frac{a}{2}} \sigma^* \sin^2 \frac{\pi x}{a}\, dx \qquad \text{B-4}$$

This integral when evaluated for the case of the dark (non-illuminated) phosphor becomes

$$T_{3D} = -j\mu_0\omega\sigma^* t \qquad \text{B-5}$$

In order to evaluate the term T_3 for the illuminated phosphor σ^* in (B-4) is replaced by $\sigma^*(x)$ from (B-3). In addition, since $\sigma(x)$ is not symmetric about $x = a/2$ the upper limit of the integral is replaced by $\frac{a+t}{2}$ while the factor 2 in B-4 is replaced by 1. Hence, B-4 for the excited phosphor becomes

$$T_{3E} = -j\mu_0\omega \int_{x=\frac{a}{2}-\frac{t}{2}}^{x=\frac{a}{2}+\frac{t}{2}} \sigma^*(x) \sin^2 \frac{\pi x}{a}\, dx$$

$$= - j\mu_0 \omega \sigma^*(0) \int_{x=\frac{a}{2}-\frac{t}{2}}^{x=\frac{a}{2}+\frac{t}{2}} e^{-n\delta\left(x-\frac{a-t}{2}\right)} \operatorname{sen}^2 \frac{\pi x}{a}\, dx$$

which becomes

$$T_{3E} = \frac{j\mu_0 \omega \sigma^*(0) a^2}{(\delta n a)^2 + 4\pi^2} \left\{ \left[(-\delta n) \operatorname{sen} \frac{\pi}{a} \frac{a+t}{2} - \frac{2\pi}{a} \cos \frac{\pi}{a} \frac{a+t}{2} \right] \left[\operatorname{sen} \frac{\pi}{a} \frac{a+t}{2} \right] - \frac{2\pi^2}{\delta n a^2} \right\} e^{-n\delta t}$$

$$- \frac{j\mu_0 \omega \sigma^*(0) a^2}{(\delta n a)^2 + 4\pi^2} \left\{ \left[(-\delta n) \operatorname{sen} \frac{\pi}{a} \frac{a-t}{2} - \frac{2\pi}{a} \cos \frac{\pi}{a} \frac{a-t}{2} \right] \left[\operatorname{sen} \frac{\pi}{a} \frac{a-t}{2} \right] - \frac{2\pi^2}{\delta n a^2} \right\} e^{-n\delta t} \qquad \text{B-6}$$

The trigonometric functions in the above may be rewritten as follows.

$$\operatorname{sen} \frac{\pi}{a} \frac{a \mp t}{2} = \pm \cos \frac{t}{2a} \pi$$

and

$$\cos \frac{\pi}{a} \frac{a \mp t}{2} = \pm \operatorname{sen} \frac{t}{2a} \pi$$

The above then reduces to

$$T_{3E} = - \frac{j\mu_0 \omega \sigma^*(0) a^2}{(\delta n a)^2 + 4\pi^2} \left\{ (-\delta n) \cos^2 \frac{t}{2a} \pi + \frac{2\pi}{a} \operatorname{sen} \frac{t}{2a} \pi \cos \frac{t}{2a} \pi - \frac{2\pi^2}{\delta n a^2} \right\} e^{-n\delta t}$$

$$- \frac{\mu_0 \omega \sigma^*(0) a^2}{(\delta n a)^2 + 4\pi^2} \left\{ - (\delta n) \cos^2 \frac{t}{2a} \pi - \frac{2\pi}{a} \cos \frac{t}{2a} \pi \operatorname{sen} \frac{t}{2a} \pi - \frac{2\pi^2}{\delta n a^2} \right\} e^{-n\delta t}.$$

Neglecting terms of third order in the expansion of the trignometric functions ($\frac{t}{2a} \ll 1$), one has

$$T_{3E} = -\frac{\jmath \mu_0 \omega \sigma^*(0)\, a^2}{(\delta n a)^2 + 4\pi^2} \left[\left(\delta n + \frac{2\pi^2}{\delta n a^2} \right) \left(1 - e^{-n\delta t} \right) + \left(\frac{\pi}{a} \right)^2 t \left(1 + e^{-n\delta t} \right) \right. \qquad \text{B-7}$$

T_{3E} as represented by (B-7) provides for the additional photoconductivity of the phosphor due to the exciting radiant energy. For the case of no absorption ($\delta = 0$) it is seen that (B-7) reduces to

$$T_{3E} = -\jmath \mu_0 \omega \sigma^*(0)\, t \qquad \text{B-8}$$

Comparing (B-7), (B-8) and (B-5), shows that $\sigma(0)$ represents the increase of photoconductivity on the surface (and also throughout the sample if $\delta = 0$) due to excitation of the phosphor.

Finally, comparison of (B-7) with II-21 and II-22 shows that $(\sigma_r - \sigma_0)\, t$ in II-21 and II-22 may be replaced by

$$\frac{\sigma^*(0)\, a^2}{(\delta n a)^2 + 4\pi^2} \left[\left(\delta n + \frac{2\pi^2}{\delta n a^2} \right) \left(1 - e^{-n\delta t} \right) + \left(\frac{\pi}{a} \right)^2 t \left(1 + e^{-n\delta t} \right) \right.$$

to account for the attenuation of the exciting radiation.

Appendix C

Sensitivity of Unbalanced Bridge

Reference is made to Equation II-28

$$V^{1/2} - V_i^{1/2} = k_1 (\sigma - \sigma_0) \qquad C-1$$

which gives the response of an unbalanced bridge. The sensitivity of the bridge is defined to be $S = V - V_i$, the change in the detector reading when the phosphor is illuminated. The balanced bridge sensitivity $S_o = V_o$, is found by letting $V_i = 0$ in the expression for bridge sensitivity. Equation (C-1) when applied to a balanced bridge becomes

$$V_0^{1/2} = k_1 (\sigma - \sigma_0) \qquad C-2$$

The unbalanced bridge sensitivity is shown to be more sensitive in the following manner. Squaring and equating the left hand side of Equations C-1 and C-2 leads to

$$V - V_i - 2V^{1/2} V_i^{1/2} + 2V_i = V_0$$

, which may be written in terms of sensitivities as

$$S = S_o + 2\left(V^{1/2} V_i^{1/2} - V_i\right)$$

$$= S_0 + 2 V_i^{1/2} \left(V^{1/2} - V_i^{1/2} \right)$$

$$= S_0 + 2 V_i^{1/2} S_0^{1/2}$$

The increase in bridge sensitivity due to unbalance is proportional to the square root of the product of the initial off balance setting (V_i) and the balanced bridge sensitivity.

References

1. K. Kalikstein, B. Kramer, and S. Gelfman, J. Appl. Phys. 39, 4252 (1968).
2. H. A. Klasens, J. Electrochem. Soc. 100, 72 (1953).
3. J. S. Prenner and F. E. Williams, J. Electrochem. Soc. 103, 342 (1956).
4. C. S. Kang, P. Beverly, P. Phipps, and R. H. Bube, Phys. Rev. 156, 998 (1967).
5. M. Schon, Z. Physik 119, 463 (1942).
6. H. A. Klasens, Nature 158, 306 (1946).
7. H. Kallmann and B. Kramer, Phys. Rev. 87, 91 (1952).
8. N. F. Mott and R. W. Gurnery, Electronic Processess in Ionic Crystals, p. 213, Oxford (1940).
9. J. Lamb and C. C. Klick, Phys. Rev. 98, 909 (1955).
10. S. Shionoya, K. Era and Y. Washizawa, J. Phys. Soc. Jap. 21, 1624 (1966).
11. R. H. Bube, Photoconductivity of Solids, Wiley, (1960).
12. A. Rose, Phys. Rev. 97, 322 (1955).
13. J. Schanda, M. Somogyi, M. Gal and G. Sziegeti, J. of Luminescence, 1,2, 51 (1970).
14. P. Lenard, S. Saeland, Ann. Phys. (Lpz), 2, 240 (1909).
15. B. Gudden and R. W. Pohl, Z. Physik 3, 98 (1920).
16. R. Frerichs, Phys. Rev. 72, 594 (1947).

17. R. Frerichs, Phys. Rev. 76, 1869 (1949).

18. R. H. Bube, Phys. Rev. 83, 393 (1951).

19. L. Gildard and H. W. Ewald, Phys. Rev. 83, 359 (1951).

20. H. Kallmann and R. Warminsky, Ann. Physik 4 69 (1948) and 4 57 (1948).

21. E. Voyatzakis, Compt. rend 209, 31 (1939).

22. J. Lamb, Phys. Rev. 90, 985 (1955).

23. H. Kallmann, B. Kramer and A. Perlmutter, Phys. Rev. 89, 700 (1953).

24. G. F. J. Garlick and A. F. Gibson, Proc. Roy. Soc. (London) AI88, 485 (1947).

25. H. Kallmann, B. Kramer and G. M. Spruch, Phys. Rev. 116, 620 (1959).

26. B. M. Jaffe and H. Kallmann, J. Am. Chem. Soc. 86, 3428 (1964).

27. A. N. Silverman, Ph.D. Thesis, New York University, (1969).

28. A. P. Ramsa, H. Jacobs and F. A. Brand, J. Appl. Phys. 30, 1054 (1959).

29. S. Deb and B. R. Nag, J. Appl. Phys. 33, 1604 (1961).

30. W. E. Bullman, B. C. Potts and R. B. Green, IRE Trans. Antennas Propagation AP-9 193 (1961).

31. A. P. Shepard, I EEE Trans. Instr. Meas. IM-15, 44 (1966).

32. J. Dziesiaty, Phys. Status Solide 6, 913 (1964).

33. K. S. Champlin, D. B. Armstrong and P. D. Gunderson Proc. I EEE 52, 677 (1964).

34. Montgomery, Technique of Microwave Measurements, 2 p. 588, Dover.

35. J. A. Curcio and C. C. Petty, J. Opt. Soc. Am. 41, 302 (1951).

36. Jackson, Classical Electrodynamics, p. 205, Wiley.

37. Sachs, Solid State Theory, p. 260, McGraw-Hill.

38. W. F. Bullman, B. C. Potts and R. B. Green, IRE Trans. Antennas Propagation, AP-9, 193 (1961)

39. H. A. Klasens, J. Phys. Chem. Solids, 7, 175 (1958).

40. R. H. Bube, Photoconductivity of Solids, p. 343, Wiley.

41. T. S. Moss, Optical Properties of Semi-Conductors, Academy Press (1956).

42. G. F. J. Garlick, Luminescent Materials, Clarendon Press (1949).

43. T. Koda and S. Shionoya, Phys. Rev. 136, A541 (1964).

44. G. Meyer, J. Phys. Chem. Solids, 7, 153 (1958).

45. N. J. Melamed, J. Electrochem. Soc. 97, 33 (1950).

46. B. Kramer and A. Turner, J. Electrochem. Soc. 110 366 (1963).

47. D. G. Thomas, J. J. Hopfield and W. M. Augustyniak, Phys. Rev. 140, A202 (1965).

48. C. B. Burgett and C. Lin, J. Phys. Chem. Solids, 31 1353 (1970).

49. Suzuki and Shionoya, J. Phys. Soc. Japan 31, 1455 (1971).

50. R. H. Sheikh and M. W. Gunn, I EEE Trans. Microwave Theory Tech. MTT-16, 117 (1968).

51. Jackson, Classical Electrodynamics, p. 245, Wiley.